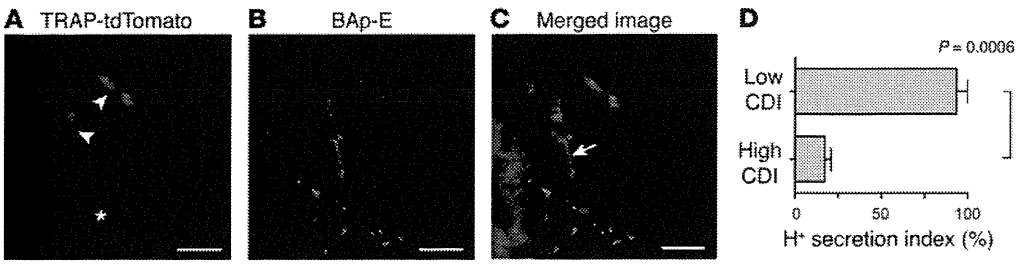

Figure 3
Visualization of bone-resorptive function of mature osteoclasts by using H^+-sensing fluorescent probe. (**A–C**) Representative images from intravital multiphoton imaging of mouse bone tissues of heterozygous TRAP-tdTomato transgenic mice treated with BAp-E, an H^+ probe detecting sites of local bone resorption (Supplemental Video 5). Mature osteoclasts expressing TRAP-tdTomato signals (**A**), green fluorescent signals from high H^+ concentration (**B**), and merged images (**C**). Green fluorescent signals from the H^+ probes overlapped with static (low CDI, arrowheads) but not moving (high CDI, asterisk) osteoclasts, suggesting that former cells are secreting protons actively and resorbing bone tissues when observed in vivo. Some green fluorescent signal (**C**, arrow) could also be detected along the bone surfaces near to static osteoclasts. Given the rate of transition from static to motile behavior of the osteoclasts, these areas are likely to be those undergoing resorption by previously static cells shortly before obtaining the image and characterizing the osteoclasts at motile. Scale bars: 40 μm. (**D**) The H^+ secretion index of mature osteoclasts. The H^+ secretion index was defined as the ratio of the number of osteoclasts overlapping with green fluorescent acid pH signals divided by the total number of osteoclasts of the indicated type that were imaged (n = 3, from 3 independent experiments).

(0.1 mg/kg), which is not sufficient for promoting osteoclastogenesis in vivo (not shown), could also efficiently convert N into R states in vivo (Figure 4D), suggesting that the level of RANKL required for N-to-R conversion may be lower than that necessary for inducing differentiation or maturation during osteoclastogenesis, with intriguing implications for control of bone state. In these experiments, unlike the cases with long exposure with RANKL (in Figure 2A), we could not observe the differences in subcellular distribution of V-type H^+-ATPases shown in Figure 1, B and C, suggesting that it may take a substantial (more than 10 to 20 minutes) period for relocalization of these proteins to support highly active bone resorption. We determined that i.v. injection of GST did not significantly change the average cell motility for up to 40 minutes (Figure 4D).

Osteoclastogenic RANKL is mainly supplied from osteoblasts, osteocytes, and/or stromal cells in bone marrow, although RANKL has also been reported to be expressed by diverse immune cell types such as T lymphocytes (24, 25). Among several T cell subtypes, $CD4^+$ Th17 cells, which are associated with autoimmune disorders including rheumatoid arthritis, have been reported to express RANKL on the cell surface (26). However, the in vivo function of RANKL on Th17 is not clear because the expressed RANKL exhibited little ability to induce osteoclastogenesis in vitro. We therefore looked for a possible physical and functional relationship between RANKL-bearing Th17 cells and mature osteoclasts in vivo by visualizing these cells simultaneously in intact bones (Figure 5A). Polyclonal Th17 and Th1 cells

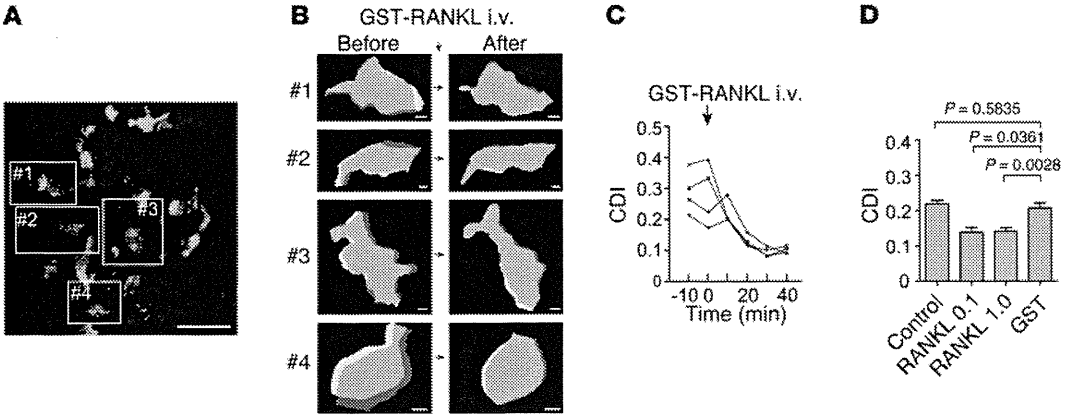

Figure 4
RANKL-mediated rapid control of mature osteoclast function. (**A**) Intravital multiphoton imaging of osteoclasts in mouse bone tissues of a3-GFP mice under control conditions (Supplemental Video 6). Mature osteoclasts expressing GFP-fused V-type H^+ ATPase a3 subunit are in green. Blue, bone surface. Cell borders are marked in white lines. Scale bar: 40 μm. (**B**) Representative computer-processed images of mature osteoclasts and their RANKL-mediated rapid shape changes. Images 1–4 were computer extracted from images under the initial condition from **A** (left panels) and again 10 minutes after i.v. injection of 1 mg/kg of GST-RANKL (right panels) (as in Figure 1, E and F). Scale bars: 5 μm. (**C**) Representative time courses of the CDI for the 4 individual cells shown in **B**. Moving (high CDI) osteoclasts underwent transition to the static (low CDI) state less than 10 minutes after i.v. administration of RANKL. (**D**) The summary of CDIs under control conditions (control) and 40 minutes after i.v. injection of 0.1 mg/kg of GST-RANKL (RANKL 0.1), 1 mg/kg of GST-RANKL (RANKL 1), or GST alone (n = 13 for control, n = 5 for 0.1 mg/kg of GST-RANKL, n = 13 for 1 mg/kg of GST-RANKL, and n = 21 for GST alone, compiled from 3 independent experiments).

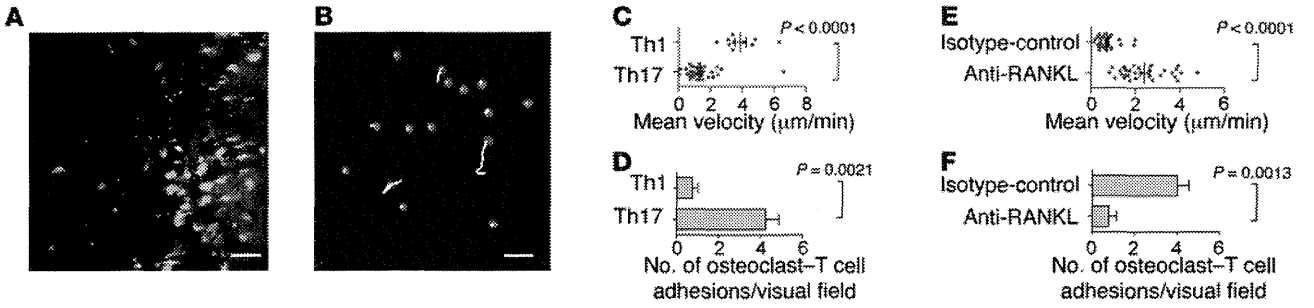

Figure 5

The interaction between Th17 and osteoclast depends on RANKL expressed on Th17. (**A**) Intravital multiphoton imaging (low-power view) of osteoclasts (green) in mouse bone tissues of a3-GFP mice after administration of in vitro–differentiated Th1 (labeled with CMF_2HC — blue) and Th17 (labeled with CMTPX — red) (Supplemental Video 7). Cell borders are marked by white lines. Scale bar: 40 μm. (**B**) The migratory behaviors of Th1 and Th17. Blue and red spheres represent Th1 and Th17 cells, respectively, and white lines show the associated trajectories. Scale bar: 40 μm. (**C**) Summary of mean tracking velocities of Th1 and Th17 cells. Data points (n = 10 for Th1, and n = 48 for Th17) represent individual cells compiled from 3 independent experiments. (**D**) The number of Th1 or Th17 cells attached to mature osteoclasts for more than 5 minutes (n = 4, from 3 independent experiments). (**E**) Summary of mean tracking velocity of Th17 cells treated with isotype control antibody or anti-RANKL antibody. Data points (n = 32 for Th17 cells treated with isotype control antibody and n = 30 for Th17 cells treated with anti-RANKL antibody) represent individual cells compiled from 3 independent experiments. (**F**) The number of Th17 cells treated with isotype control antibody or anti-RANKL antibody attached to mature osteoclasts for more than 5 minutes (n = 5, from 3 independent experiments).

were differentiated in vitro using appropriate sets of cytokines and neutralizing antibodies (ref. 26 and Supplemental Figure 4), stained with cell-permeable fluorescent dyes, CMTPX (red) and CMF_2HC (blue), respectively, and then adoptively transferred i.v. into a3-GFP mice shortly before imaging (Figure 5, A and B, and Supplemental Video 7). Th17, but not Th1, preferentially adhered to mature osteoclasts (Figure 5, C and D) under these conditions, even though both Th cells migrated into bone marrow cavity to the same extent (Supplemental Figure 5A). Pretreatment of Th17 with anti-RANKL neutralizing antibody (27, 28) or osteoprotegerin (OPG), a decoy receptor for RANKL (29), reduced association of these T cells with the osteoclasts (Figure 5, E and F, Supplemental Figure 6, and Supplemental Video 8), whereas we observed no effect of anti-RANKL on the mobility of Th1 cells (Supplemental Figure 7). These results suggest that the interaction between Th17 and osteoclast is at least partly dependent on RANKL expressed on the surface of Th17, although we cannot exclude the possibility that additional molecules may play a role in this colocalization. Moreover, we found that mature osteoclasts adherent to Th17 were R, as compared with nonconjugated cells (Figure 6, A and C), and that N osteoclasts were converted to static ones shortly after conjugation with Th17 (Figure 6, D–F, and Supplemental Video 9).

We further examined the role of Th17 in osteoclastic bone resorption using the pH probe (BAp-E) to detect local pH changes in vivo (Figure 3). Either Th17 or Th1 cells were labeled with CMTPX (red) and then transferred to the mice pretreated with BAp-E. Th17 cells seemed to be closely adjacent to green signals from BAp-E representing acidic areas (Figure 6G), whereas Th1 cells were not present in proximity to these indicator signals (Figure 6G). Figure 6H shows the ratio of the number of Th1 or Th17 cells close to the low pH signals divided by the total number of Th1 or Th17 cells in visual fields. These data indicate a preferential association between the location of Th17 T cells and sites of pH drop and support our concept that Th17, but not Th1, mediates bone-resorptive acid secretion from mature osteoclasts at local sites of T cell–osteoclast contact. Taken together, these results reveal a new function of RANKL-expressing Th17, namely stimulation of bone resorption by converting nonresorbing to resorbing mature osteoclasts on the bone surface in situ.

Discussion

Bone tissue sectioning accompanied with conventional histomorphometric analyses has been the major methodology employed to date for studying bone resorption and osteoclast function in vivo (30) and has provided substantial insight into functional aspects of bone physiology. Here we applied 2-photon microscopy to attain previously unavailable insight into the in vivo dynamic behavior of osteoclasts on the bone surface, detailing for what we believe is the first time how osteoclast movement and resorptive function are related as well as how this activity is modulated by cytokines, immune cells, and pharmacologic agents. Our imaging studies have revealed that osteoclasts on the bone surface show substantial heterogeneity in motility and rapid transitions in this motility in conjunction with alternation in their functional states. RANKL administration or direct interaction with RANKL-bearing Th17 cell appears to stimulate local bone resorption by dynamically modulating the linked changes in migratory status and function of osteoclasts within a short period (10~20 minutes).

While it provides information on osteoclast behavior and activity in situ, data from this method must be compared with caution to results derived from other techniques. Previous studies using conventional bone histomorphometry showed that bisphosphonate treatment stimulates osteoclast formation in mice (31), findings that are in seeming conflict with the present results shown in Figure 2C. Our own studies using bone sectioning with TRAP staining to examine the effect of risedronate in a3-GFP mice have also shown that the total number of mature osteoclasts slightly increased, compared with control conditions (not shown). Moreover, we could find some larger a3-GFP$^+$TRAP$^+$ double-positive osteoclasts in treated mice, in accord with previous results demonstrating an increase in giant osteoclasts in bisphosphonate-treated bone specimens (31). Multiphoton imaging, as we use it here, provides 2D scanning on the bone

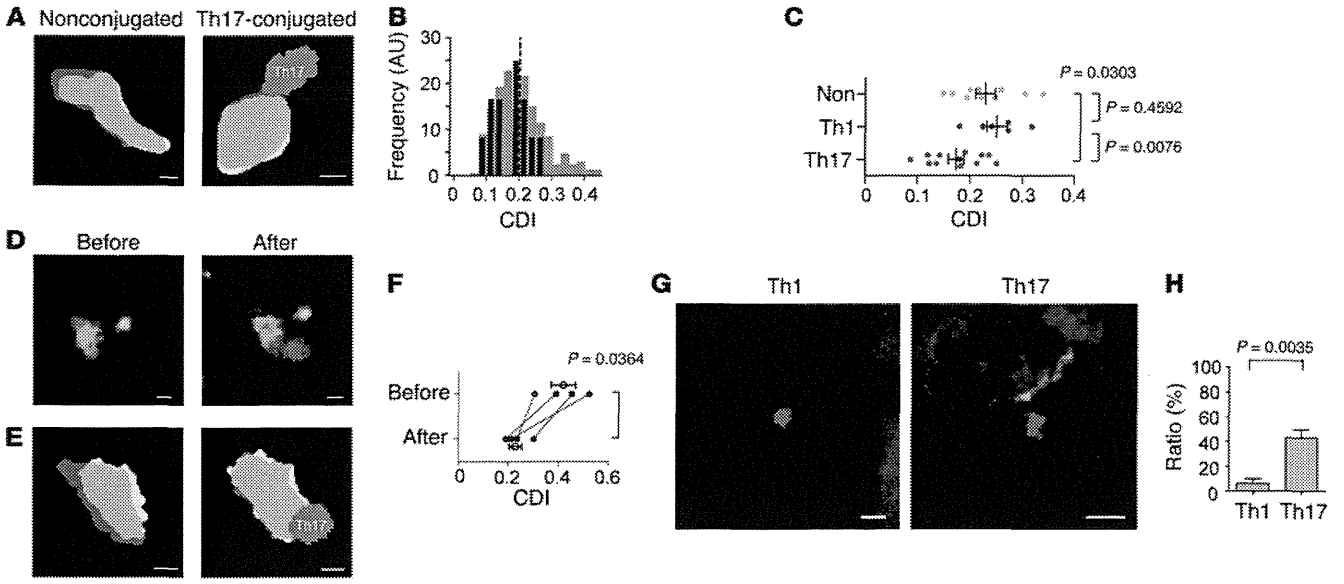

Figure 6

Regulation of mature osteoclast function by RANKL expressed on Th17. (**A**) Mature osteoclasts (green/red/yellow) either alone or in conjugate with Th17 (magenta); corresponding CDIs were determined (see details in Figure 1D). Scale bars: 5 μm. (**B**) Histogram of CDIs of mature osteoclasts conjugated with Th17 (black) and under control conditions (gray, same as in Figure 1H). (**C**) Summary of the CDIs of mature osteoclasts alone or conjugated with Th1 or Th17 (n = 10 for nonconjugated [Non], n = 6 for Th1-conjugated [Th1], and n = 12 for Th17-conjugated [Th17]). (**D**) A representative image showing a migrating Th17 contacting a mature osteoclast. Green, mature osteoclast; red, Th17. Scale bar: 5 μm. (**E**) Change in osteoclast motility associated with Th17 contact. The CDIs before (left) and after (right) conjugation with Th17 are depicted. Magenta, Th17. Scale bars: 5 μm. (**F**) Summary of CDI changes corresponding to Th17 conjugation (n = 4). Moving (high CDI) osteoclasts underwent transition into static (low CDI) states 20 minutes after conjugation with Th17. (**G**) Representative images of live bone imaging of wild-type mice treated with BAp-E. In vitro–differentiated Th1 (left) or Th17 (right) were labeled with CMTPX (red) and then transferred as independent. Fluorescent signals from high H^+ concentration are in green. Blue, bone surface. Scale bar: 10 μm. (**H**) The ratio of the number of Th1 or Th17 attached to the BAp-E divided by the total number of Th1 or Th17 (n = 4). Each experiment was performed independently at least 3 times.

surface in a focal plane, whereas the bone surface is represented by 1D "lines" along the bone trabeculae in classical histomorphometrical analyses. Cell shapes and the appearance of mature osteoclasts in these 2 analysis systems are quite different. Perhaps of greatest importance is that the present imaging method specifically detects only those osteoclasts tightly adherent to the bone surface and not cells that may be near this surface but not firmly bound. The majority of mature osteoclasts in bisphosphonate-treated mice may be slightly detached from the surface (32) and thus not quantified in our imaging. These considerations suggest a cautious approach to interpretation of all imaging data; in the present case, the method is best suited to the dynamic and functional analysis of strongly bone adherent osteoclasts and not all such cells in the marrow, and our interpretations are based on this adherent subpopulation.

RANKL is generally considered to be a critical factor in the terminal differentiation of osteoclasts. Here, we show RANKL also plays roles in regulating the bone-resorptive function of fully differentiated "mature" osteoclasts (Supplemental Figure 8). This finding is consistent with maintenance of expression of RANK, a receptor for RANKL, on mature osteoclasts. This contrasts with expression of CSF1R or CX_3CR1, which is necessary for differentiation or positioning of osteoclasts and their precursors, but becomes dispensable in the late phase of osteoclastogenesis and which is downregulated after maturation. Importantly, this newly identified effect of RANKL is seen with a lower amount of RANKL than that required for stimulating de novo osteoclastogenesis, and it appears that the amount expressed on Th17 is indeed sufficient for this effect. There have been a series of reports indicating a critical contribution of Th17 in bone-resorptive inflammatory diseases, such as rheumatoid arthritis, although the molecular mechanism by which these T cells contribute to pathogenesis has been unresolved (33, 34). Th17 accumulation in synovial fluid (35) may contribute to arthritic bone erosion partly by stimulating mature osteoclasts in such a manner. Overall, our findings clearly demonstrate an unanticipated cycling of mature osteoclasts between active, bone-resorptive and static, inactive states as well as key molecular and cellular players involved in changing the relative proportion of the 2 osteoclast types at the bone surface. This resorption switching on the bone surface in situ may represent an interesting therapeutic target.

Methods

Mice. The generation of the V-type H^+ ATPase a3 subunit-GFP fusion knockin mice was described previously (13). For the generation of the TRAP promoter-tdTomato transgenic mice, tdTomato cDNA (Clontech) was inserted into an pL451 vector containing an Frt-PGK-promoter-Neo-Frt cassette. Recombination protocol was carried out as described (36). Briefly, forward primer (5′-TAGTGCCTGAGTTTATAGGCATGCACCGTGAGACCAGGCTCAGCGGGCTAGTCTTTCTTTGCTTGGACCAGGGTCTCGCTCTCTGTCCTCACCAGAGACTCTGAACTCCCTCTCTTCCTCACAG**ATG**GTGAGCAAGGGCGAGGAGGTCA-3′) and reverse primer (5′-CATTGGGGACCCCTCCCCAGTCGCCCACAGCCACAAATCTCAGGGTGGGAGTGGGGGCTGTACCGTGGGTCAG-

GAGTGGGAGCCATATGATTTGTAGGCCCAGCAGCACCACCCATGAATCAGTTATATTATGTACCTGACTGAT-3′) were used to amplify a fragment containing tdTomato cDNA as well as the homologous sequences flanking the mouse TRAP ATG start codon site. The underlined sequences of these primers were matching to the sequences before and after the start codon ATG (bold) of TRAP. The resulting PCR product was transfected into the SW105 bacteria carrying RP24-75C9 according to the standard procedure as described previously. The kanamycin-resistant clones were further screened using PCR screening protocols. The Frt-PGK-promoter-Neo-Frt cassette in positive BAC clones was deleted by inducing FLP recombinase followed by confirmation using BAC DNA sequencing (Supplemental Figure 9). The purified RP24-75C9-TRAP-tdTomato was microinjected into the pronucleus of C57BL/6 fertilized eggs. Southern blot was employed to identify the potential founder mice using a tdTomato DNA fragment as a probe. A DNA dot bolt was carried out to determine the specificity of this tdTomato probe using the plasmids containing tdTomato or other cDNA. All mice were bred and maintained under specific pathogen-free conditions at animal facilities of Osaka University and NIH. We confirmed that both a3-GFP knockin and TRAP-tdTomato transgenic mice had no abnormality in terms of bone homeostasis by using bone morphometrical analyses.

Multiphoton intravital bone tissue imaging. Intravital microscopy of mouse calvaria bone tissues was performed using a protocol modified from a previous study (7, 8). Ten- to fourteen-week-old mice were anesthetized with isoflurane (Escain; 2.0% vaporized in 100% oxygen), the frontoparietal regions of the skull bones were exposed, and then the internal surfaces of bones adjacent to bone marrow cavity were observed by using multiphoton excitation microscopy. The imaging system was composed of a multiphoton microscope (SP5; Leica) driven by a laser (Mai-Tai HP Ti: Sapphire; Spectraphysics) tuned to 840–900 nm and an upright microscope (DM6000B; Leica) equipped with a ×20 water immersion objective (HCX APO, N.A. 1.0; Leica). Fluorescent cells were detected through band-pass emission filters at 525/50 nm (for GFP and BAp-E), at 455/50 nm (for CMF_2HC), and at 585/40 nm (for CMTPX). Vessels were visualized by injecting 70 kDa of Texas red–conjugated dextran (detected using a 585/40 nm filter) i.v. immediately before imaging. Image stacks were collected at 5-μm vertical step size at a depth of 100–150 μm below the skull bone surface. Raw imaging data was processed with Imaris (Bitplane) with a Gaussian filter for noise reduction. Image drifts were corrected by using image analysis software, Imaris or CL-Quant 2.30 (Nikon), according to a standard protocol.

Chemical synthesis of H^+ sensing fluorescent probe. The chemical synthesis of BAp-E, a fluorescent probe detecting H^+ secretion was described previously (21).

Image data analysis. Assessment of the R state and N state of mature osteoclasts was performed by using newly developed image analysis software CL-Quant 2.30 (Nikon) (37) for tracking the morphological changes of mature osteoclasts. The details of how we defined the R and N states are described in Supplemental Figure 2 and Supplemental Video 2.

Treatment with RANKL and bisphosphonate. In some experiments, a3-GFP mice were treated with GST-RANKL and/or risedronate. GST-RANKL (Oriental Yeast) (1 mg/kg) dissolved in PBS was injected intraperitoneally into a3-GFP female mice 2 days before imaging. 10 μg/kg of risedronate (17) (provided by Ajinomoto Pharmaceuticals Co.) dissolved in PBS was subcutaneously injected into the mice every day beginning 5 days prior to taking images. GST (1 mg/kg) dissolved in PBS was also injected as a control. For examining short-term effects of RANKL, GST-RANKL (1 or 0.1 mg/kg) or GST (1 mg/kg) dissolved in PBS were administered i.v. during imaging, and images were acquired consecutively.

In vitro differentiation of $CD4^+$ T cells. $CD4^+$ T cells were purified from the spleen and peripheral lymph nodes of wild-type mice by using Dynabeads FlowComp Mouse $CD4^+$ Isolation Kit (Life Technologies). The purity of the $CD4^+$ T cells was greater than 95%. These $CD4^+$ T cells were cultured with a plate-bound 1 μg/ml anti-CD3 mAb (Biolegend) and 1 μg/ml anti-CD28 mAb (Biolegend) and differentiated into Th1 or Th17 cells, in the presence of 10 μg/ml anti–IL-4 mAb (R&D) and 10 ng/ml IL-12 (PeproTech), or 10 μg/ml anti–IFN-γ mAb (R&D), 10 μg/ml anti–IL-4 mAb, and 10 ng/ml IL-23 (R&D), respectively. After incubation for 3 days, cells were collected and checked for differentiation into Th1 or Th17, by using flow cytometry and RT-PCR. In vitro differentiated Th1 or Th17 cells were labeled with CMF_2HC (50 μM; Life Technologies) and CMTPX (15 μM; Life Technologies), respectively. In some experiments, Th1 or Th17 cells were incubated with 1 μg/ml anti-mouse RANKL neutralizing mAb (Oriental Yeast), OPG (R&D), or rat IgG2a, κ isotype control antibody (BD Biosciences – Pharmingen) at 4°C for 15 minutes and labeled with CMTPX (15 μM) or CMF_2HC (50 μM). After labeling, each cell was transferred to a3-GFP mice. Two hours, later mouse skull bone tissues were observed by using intravital multiphoton microscopy, as previously described.

Immunohistochemistry. Immunohistological analyses were performed as described previously (7). Fluorescence-based staining for TRAP with ELF97 substrate (Life Technologies) was used with some modifications.

Quantitative real-time PCR. Quantitative real-time PCR was performed with Thermal Cycler Dice Real Time System TP800 (Takara) using the following specific primer pairs: Rorγt (5′-GCCGCGGAGCAGACACACTT-3′ and 5′-GCTGCAGCCCAAGGCTCGAA-3′), RANKL (5′-GTACCTGCGCAGCTCGGAGG-3′ and 5′-GCCTCAGGCTTGCCTCGCTG-3′), and GAPDH (5′-ACCACAGTCCATGCCATCAC-3′ and 5′-TCCACCACCCTGTTGCTGTA-3′).

Flow cytometry. All reagents were purchased from BD. To examine the existence of transferred Th1 and Th17 cells in spleen and bone marrow of a3-GFP mice, splenocytes and bone marrow cells were collected from the mice after taking images. To confirm the cell-surface expression of RANKL on T cells, in vitro differentiated Th1 and Th17 cells were first incubated with anti-mouse CD16/32 antibody (eBioscience) to block nonspecific binding, followed by incubation with either PE-conjugated rat anti-mouse RANKL antibody (BD Pharmingen) or PE-conjugated rat IgG2a, κ isotype control (BioLegend). Flow cytometric data were collected on a FACSCanto II (BD) and analyzed with FlowJo software (Tree Star).

Statistics. The Mann–Whitney rank sum test was used to calculate *P* values for highly skewed distributions. For Gaussian-like distributions, 2-tailed *t* tests were used. Data represent mean ± SEM unless otherwise specified. $P < 0.05$ was considered significant.

Study approval. All animal experiments were performed according to institutional animal experimental guidelines under approved protocols from the Animal Experimental Committee of Osaka University and the National Institute of Allergy and Infectious Diseases (NIAID) Institutional Animal Care and Use Committee.

Acknowledgments

We thank Y. Shimazu and A. Kubo for experimental assistance. This work was supported by Grants-in-Aid for Encouragement of Young Scientists (A) (no. 22689030), for Scientific Research on Innovative Areas (no. 22113007); by a Funding Program for World-Leading Innovative R&D on Science and Technology (FIRST Program) from the Ministry of Education, Science, Sports and Culture of Japan; by a Grant-in-Aid for Research on Allergic Disease and Immunology (H21-010) from the Ministry of Health, Labor and Welfare of Japan; by a grant from the International Human Frontier Science Program (CDA-00059/2009 and RGY0077/2011); and by grants from the Takeda Science Founda-

tion, the Mochida Memorial Foundation for Medical and Pharmaceutical Research, the Astellas Foundation for Research on Metabolic Disorders, the Kanae Foundation for the Promotion of Medical Science, the Pfizer Health Research Foundation, and the Uehara Memorial Foundation. It was also supported by the Intramural Research Program, NIAID, NIH.

Received for publication September 28, 2012, and accepted in revised form November 29, 2012.

Address correspondence to: Masaru Ishii, Laboratory of Cellular Dynamics, Immunology Frontier Research Center, Osaka University, 3-1 Yamada-oka, Suita, Osaka 565-0871, Japan. Phone: 81.6.6879.4268; Fax: 81.6.6879.8296; E-mail: mishii@ifrec.osaka-u.ac.jp.

Ge-Hong Sun-Wada's present address is: Department of Biochemistry, Faculty of Pharmaceutical Sciences, Doshisha Women's College, Kyoto, Japan.

1. Teitelbaum SL, Ross FP. Genetic regulation of osteoclast development and function. *Nat Rev Genet.* 2003;4(8):638–649.
2. Karsenty G, Wagner EF. Reaching a genetic and molecular understanding of skeletal development. *Dev Cell.* 2002;2(4):389–406.
3. Takahashi N, et al. Osteoclast-like cell formation and its regulation by osteotropic hormones in mouse bone marrow cultures. *Endocrinology.* 1988; 122(4):1373–1382.
4. Roodman GD, Windle JJ. Paget disease of bone. *J Clin Invest.* 2005;115(2):200–208.
5. Turcotte RE. Giant cell tumor of bone. *Orthop Clin North Am.* 2006;37(1):35–51.
6. Mazo IB, et al. Bone marrow is a major reservoir and site of recruitment for central memory CD8+ T cells. *Immunity.* 2005;22(2):259–270.
7. Ishii M, et al. Sphingosine-1-phosphate mobilizes osteoclast precursors and regulates bone homeostasis. *Nature.* 2009;458(7237):524–528.
8. Ishii M, Kikuta J, Shimazu Y, Meier-Schellersheim M, Germain RN. Chemorepulsion by blood S1P regulates osteoclast precursor mobilization and bone remodeling in vivo. *J Exp Med.* 2010; 207(13):2793–2798.
9. Blair HC, Teitelbaum SL, Ghiselli R, Gluck S. Osteoclastic bone resorption by a polarized vacuolar proton pump. *Science.* 1989;245(4920):855–857.
10. Nakamura H, Moriyama Y, Futai M, Ozawa H. Immunohistochemical localization of vacuolar H(+)-ATPase in osteoclasts of rat tibiae. *Arch Histol Cytol.* 1994;57(5):535–539.
11. Toyomura T, Oka T, Yamaguchi C, Wada Y, Futai M. Three subunit a isoforms of mouse vacuolar H(+)-ATPase. Preferential expression of the a3 isoform during osteoclast differentiation. *J Biol Chem.* 2000; 275(12):8760–8765.
12. Toyomura T, et al. From lysosomes to the plasma membrane: localization of vacuolar-type H+ -ATPase with the a3 isoform during osteoclast differentiation. *J Biol Chem.* 2003;278(24):22023–22030.
13. Sun-Wada GH, Tabata H, Kawamura N, Aoyama M, Wada Y. Direct recruitment of H+-ATPase from lysosomes for phagosomal acidification. *J Cell Sci.* 2009;122(pt 14):2504–2513.
14. Nishi T, Forgac M. The vacuolar (H+)-ATPases — nature's most versatile proton pumps. *Nat Rev Mol Cell Biol.* 2002;3(2):94–103.
15. Frattini A, et al. Defects in TCIRG1 subunit of the vacuolar proton pump are responsible for a subset of human autosomal recessive osteopetrosis. *Nat Genet.* 2000;25(3):343–346.
16. Karsdal MA, Martin TJ, Bollerslev J, Christiansen C, Henriksen K. Are nonresorbing osteoclasts sources of bone anabolic activity? *J Bone Miner Res.* 2007;22(4):487–494.
17. Tomimori Y, et al. Evaluation of pharmaceuticals with a novel 50-hour animal model of bone loss. *J Bone Miner Res.* 2009;24(7):1194–1205.
18. Soysa NS, et al. The pivotal role of the alternative NF-kappaB pathway in maintenance of basal bone homeostasis and osteoclastogenesis. *J Bone Miner Res.* 2010;25(4):809–818.
19. Reszka AA, Rodan GA. Mechanism of action of bisphosphonates. *Curr Osteoporos Rep.* 2003; 1(2):45–52.
20. Russell RG, et al. Bisphosphonates: an update on mechanisms of action and how these relate to clinical efficacy. *Ann N Y Acad Sci.* 2007;1117:209–257.
21. Kowada T, et al. In vivo fluorescence imaging of bone-resorbing osteoclasts. *J Am Chem Soc.* 2011; 133(44):17772–17776.
22. Nakayama T, et al. Polarized osteoclasts put marks of tartrate-resistant acid phosphatase on dentin slices — a simple method for identifying polarized osteoclasts. *Bone.* 2011;49(6):1331–1339.
23. Burgess TL, et al. The ligand for osteoprotegerin (OPGL) directly activates mature osteoclasts. *J Cell Biol.* 1999;145(3):527–538.
24. Kong YY, et al. Activated T cells regulate bone loss and joint destruction in adjuvant arthritis through osteoprotegerin ligand. *Nature.* 1999; 402(6759):304–309.
25. Takayanagi H, et al. T-cell-mediated regulation of osteoclastogenesis by signalling cross-talk between RANKL and IFN-gamma. *Nature.* 2000; 408(6812):600–605.
26. Sato K, et al. Th17 functions as an osteoclastogenic helper T cell subset that links T cell activation and bone destruction. *J Exp Med.* 2006; 203(12):2673–2682.
27. Asselin-Labat ML, et al. Control of mammary stem cell function by steroid hormone signalling. *Nature.* 2010;465(7299):798–802.
28. Furuya Y, et al. Increased bone mass in mice after single injection of anti-receptor activator of nuclear factor-kappaB ligand-neutralizing antibody: evidence for bone anabolic effect of parathyroid hormone in mice with few osteoclasts. *J Biol Chem.* 2011; 286(42):37023–37031.
29. Simonet WS, et al. Osteoprotegerin: a novel secreted protein involved in the regulation of bone density. *Cell.* 1997;89(2):309–319.
30. Parfitt AM, et al. Bone histomorphometry: standardization of nomenclature, symbols, and units. Report of the ASBMR Histomorphometry Nomenclature Committee. *J Bone Miner Res.* 1987;2(6):595–610.
31. Matsumoto T, et al. Distinguishing the proapoptotic and antiresorptive functions of risedronate in murine osteoclasts: role of the Akt pathway and the ERK/Bim axis. *Arthritis Rheum.* 2011; 63(12):3908–3917.
32. Kuroshima S, Go VA, Yamashita J. Increased numbers of nonattached osteoclasts after long-term zoledronic acid therapy in mice. *Endocrinology.* 2012;153(1):17–28.
33. Adamopoulos IE, Bowman EP. Immune regulation of bone loss by Th17 cells. *Arthritis Res Ther.* 2008; 10(5):225.
34. Peck A, Mellins ED. Breaking old paradigms: Th17 cells in autoimmune arthritis. *Clin Immunol.* 2009;132(3):295–304.
35. Takayanagi H. Osteoimmunology and the effects of the immune system on bone. *Nat Rev Rheumatol.* 2009;5(12):667–676.
36. Lee EC, et al. A highly efficient Escherichia coli-based chromosome engineering system adapted for recombinogenic targeting and subcloning of BAC DNA. *Genomics.* 2001;73(1):56–65.
37. Alworth SV, Watanabe H, Lee JS. Teachable, high-content analytics for live-cell, phase contrast movies. *J Biomol Screen.* 2010;15(8):968–977.

HEPATOLOGY
Official Journal of the American Association for the Study of Liver Diseases

Hepatitis C Virus NS4B Protein Targets STING and Abrogates RIG-I–Mediated Type I Interferon-Dependent Innate Immunity

Sayuri Nitta,[1*] Naoya Sakamoto,[1,2,6*] Mina Nakagawa,[1,2] Sei Kakinuma,[1,2] Kako Mishima,[1] Akiko Kusano-Kitazume,[1] Kei Kiyohashi,[1] Miyako Murakawa,[1] Yuki Nishimura-Sakurai,[1] Seishin Azuma,[1] Megumi Tasaka-Fujita,[1] Yasuhiro Asahina,[1,2] Mitsutoshi Yoneyama,[3] Takashi Fujita,[4,5] and Mamoru Watanabe[1]

Hepatitis C virus (HCV) infection blocks cellular interferon (IFN)-mediated antiviral signaling through cleavage of Cardif by HCV-NS3/4A serine protease. Like NS3/4A, NS4B protein strongly blocks IFN-β production signaling mediated by retinoic acid–inducible gene I (RIG-I); however, the underlying molecular mechanisms are not well understood. Recently, the stimulator of interferon genes (STING) was identified as an activator of RIG-I signaling. STING possesses a structural homology domain with flaviviral NS4B, which suggests a direct protein-protein interaction. In the present study, we investigated the molecular mechanisms by which NS4B targets RIG-I–induced and STING-mediated IFN-β production signaling. IFN-β promoter reporter assay showed that IFN-β promoter activation induced by RIG-I or Cardif was significantly suppressed by both NS4B and NS3/4A, whereas STING-induced IFN-β activation was suppressed by NS4B but not by NS3/4A, suggesting that NS4B had a distinct point of interaction. Immunostaining showed that STING colocalized with NS4B in the endoplasmic reticulum. Immunoprecipitation and bimolecular fluorescence complementation (BiFC) assays demonstrated that NS4B specifically bound STING. Intriguingly, NS4B expression blocked the protein interaction between STING and Cardif, which is required for robust IFN-β activation. NS4B truncation assays showed that its N terminus, containing the STING homology domain, was necessary for the suppression of IFN-β promoter activation. NS4B suppressed residual IFN-β activation by an NS3/4A-cleaved Cardif (Cardif1-508), suggesting that NS3/4A and NS4B may cooperate in the blockade of IFN-β production. *Conclusion*: NS4B suppresses RIG-I–mediated IFN-β production signaling through a direct protein interaction with STING. Disruption of that interaction may restore cellular antiviral responses and may constitute a novel therapeutic strategy for the eradication of HCV. (HEPATOLOGY 2013;57:46-58)

Type I interferon (IFN) plays a central role in eliminating hepatitis C virus (HCV) both under physiological conditions and when used as a therapeutic intervention.[1-3] In experimental acute-resolving HCV infection in chimpanzees, numerous IFN-related genes are expressed during clinical course of infection.[4] Viruses are recognized by cellular innate immune receptors, such as toll-like receptors, and a family of RIG-I–like receptors, such as retinoic-acid-inducible gene I (RIG-I) and melanoma-differentiation-associated gene 5 (MDA-5); host antiviral responses are then activated, resulting in the

From the [1]Departments of Gastroenterology and Hepatology; [2]Departments of Hepatitis Control, Tokyo Medical and Dental University, Tokyo, Japan; [3]Division of Molecular Immunology, Medical Mycology Research Center, Chiba University, Chiba, Japan; [4]Laboratory of Molecular Genetics, Department of Genetics and Molecular Biology, Institute for Virus Research, Kyoto University, Kyoto, Japan; [5]Laboratory of Molecular Cell Biology, Graduate School of Biostudies, Kyoto University, Kyoto, Japan; and [6]Department of Gastroenterology and Hepatology, Hokkaido University, Hokkaido, Japan.

Received September 16, 2011; accepted July 24, 2012.

BiFC, bimolecular fluorescence complementation; CARD, caspase recruitment domain; DAPI, 4',6-diamidino-2-phenylindole; dsRNA, double-stranded RNA; ER, endoplasmic reticulum; FACL4, fatty acid-CoA ligase, long chain 4; HCV, hepatitis C virus; IFN, interferon; IKKε, IκB kinase ε; IRF-3, interferon-regulatory factor 3; ISRE, interferon-stimulated response element; MAM, mitochondria-associated ER membrane; mKG, monomeric Kusabira-Green; PDI, protein disulphide-isomerase; pIRF-3, phosphorylated IRF3; poly(dA:dT), poly(deoxyadenylic-deoxythymidylic) acid; RIG-I, retinoic acid–inducible gene I; siRNA, small interfering RNA; SOCS, suppressor of cytokine signaling; STAT1, signal transducer and activator of transcription protein-1; STING, stimulator of interferon genes; TBK1, TANK binding kinase 1.

**These authors contributed equally to this work.*

production of cytokines such as type I and type III IFNs.[5] RIG-I is activated through recognition of short double-strand RNA (dsRNA) or triphosphate at the 5′ end of dsRNA as pathogen-associated molecular patterns,[6,7] forming a homo-oligomer that binds with the caspase recruitment domain (CARD) of Cardif (also known as MAVS, VISA, or IPS-1).[8-11] Cardif subsequently recruits TANK binding kinase 1 (TBK1) and IκB kinase ϵ (IKKϵ) kinases, which catalyze phosphorylation and activation of IFN regulatory factor-3 (IRF-3).[12] Activation of TBK1 and IKKϵ results in the phosphorylation of IRF-3 or IRF-7, translocation to the nucleus, and induction of IFN-β mRNA transcription.

Several HCV proteins can block host cellular antiviral responses. HCV core protein blocks IFN signaling by interacting with signal transducer and activator of transcription protein-1 (STAT1).[13] The core protein also induces expression of suppressor of cytokine signaling-1 (SOCS1) and SOCS3, and blocks Janus kinase–STAT signaling.[14,15] A well-elucidated immune evasion strategy of HCV involves NS3/4A serine protease and its ability to inhibit host IFN signal pathways. Gale and colleagues[11,16,17] revealed that NS3/4A protease cleaves Cardif at Cys-508 resulting in dislocation of Cardif from mitochondria, and blocks downstream signaling of IFN-β production. On the other hand, Baril et al.[18] reported that Cardif was still able to form a homo-oligomer and to activate downstream IFN production signaling despite delocalization from the mitochondria. These reports suggest that homo-oligomerization of Cardif, and not mitochondrial anchorage, is essential for the activation of downstream IFN signaling and that other virus-derived molecules may cooperate with NS3/4A to abrogate the signaling of IFN production.

We reported previously that HCV-NS4B, as well as NS3/4A, inhibited RIG-I and Cardif-mediated interferon-stimulated response element (ISRE) activation, while TBK1- and IKKϵ-mediated ISRE activation were not suppressed.[19] These results indicate that NS4B suppresses IFN production signaling by targeting Cardif or other unknown signaling molecules between the level of Cardif and TBK1/IKKϵ.

Recently, a stimulator of interferon genes (STING, also known as MITA/ERIS/MPYS/TMEM173) was identified as a positive regulator of RIG-I–mediated IFN-β signaling.[20-23] STING is a 42-kDa protein localized predominantly in the endoplasmic reticulum (ER) that binds RIG-I, Cardif, TBK1, and IKKϵ. STING is thought to act as a scaffold for Cardif/TBK1/IRF-3 complex upon viral infection.[22] It has been reported that NS4B of yellow fever virus, which is a member of the flaviviridae family of viruses, inhibits its STING activation probably through a direct molecular interaction.[24] These reports have led us postulate that HCV-NS4B may also inhibit RIG-I dependent IFN signaling through association with STING.

In the present study, we further investigated the molecular mechanisms by which HCV-NS4B protein inhibits RIG-I–mediated IFN expression signaling. We demonstrated that HCV-NS4B specifically binds STING, blocks the molecular interaction between STING and Cardif, and suppresses the RIG-I–like receptor–induced activation of IFN-β production signaling.

Materials and Methods

Plasmids. The ΔRIG-I and RIG-IKA plasmids express constitutively active and inactive RIG-I, respectively.[5] Full-length Cardif (Cardif) and CARD-truncated Cardif (ΔCARD) plasmids were provided by J. Tschopp.[11] Plasmids expressing STING were provided by G. N. Barber.[20] Plasmids expressing HCV NS3/4A, NS4B, and truncated NS4B have been described.[25] Plasmid pIFNβ-Fluc was provided by R. Lin.[26]

Cell Culture. HEK293T and Huh7 cells were maintained in Dulbecco's modified minimal essential medium (Sigma) supplemented with 2 mM L-glutamine and 10% fetal calf serum at 37°C with 5% CO_2.

HCV Replicon Constructs and HCV-JFH1 Cell Culture. An HCV subgenomic replicon plasmid, pRep-Feo, expressed fusion protein of firefly luciferase and neomycin phosphotransferase.[27,28] Huh7 cells were transfected by Rep-Feo RNA, cultured in the presence of 500 μg/mL of G418, and a cell line that stably expressed Feo replicon was established. For HCV cell culture, the HCV-JFH1 strain was used.[29,30]

Antibodies. Antibodies used were anti–IRF-3 (FL-425, Santa Cruz Biotechnology), anti-HA (Invitrogen), anti-myc (Invitrogen), mouse anti-PDI (Abcam),

Address reprint requests to: Naoya Sakamoto, M.D., Ph.D., Department of Gastroenterology and Hepatology, Hokkaido University, Kita15, Nishi8, Kita-ku, Sapporo, Hokkaido, 060-0808, Japan. E-mail: nsakamoto.gast@tmd.ac.jp; fax (81)-11-706-8036.

View this article online at wileyonlinelibrary.com.

DOI 10.1002/hep.26017

Potential conflict of interest: Nothing to report.

Additional Supporting Information may be found in the online version of this article.

rabbit anti-PDI (Enzo Life Science), anti-Flag (Sigma Aldrich), anti-Cardif (Enzo Life Science), anti-phospho–IRF-3 (Ser396, Millipore), anti-monomeric Kusabira-Green C- or N-terminal fragment (MBL), and anti-FACL4 (Abgent).

Luciferase Reporter Assay. IFN-β reporter assays were performed as described.[19,31] The plasmids pIFN-β-Fluc and pRL-CMV were cotransfected with NS3/4A or NS4B, and ΔRIG-I, Cardif, STING or poly(deoxyadenylic-deoxythymidylic) acid [poly(dA:dT)] (Invivogen). RIG-IKA, ΔCARD, and pcDNA3.1, respectively, were used as controls. Luciferase assays were performed 24 hours after transfection by using a 1420 Multilabel Counter (ARVO MX PerkinElmer) and Dual Luciferase Assay System (Promega). Assays were performed in triplicate, and the results are expressed as the mean ± SD.

Immunoblotting. Preparation of total cell lysates was performed as described.[19,28] Protein was separated using NuPAGE 4%-12% Bis/Tris gels (Invitrogen) and blotted onto an Immobilon polyvinylidene difluoride membrane. The membrane was immunoblotted with primary followed by secondary antibody, and protein was detected by chemiluminescence.

Immunoprecipitation Assay. HEK-293T or Huh7 cells were transfected with plasmids as indicated. Twenty-four hours after transfection, cellular proteins were harvested and immunoprecipitation assays were performed using an Immunoprecipitation Kit according to the manufacturer's protocol (Roche Applied Science). The immunoprecipitated proteins were analyzed by immunoblotting.

Indirect Immunofluorescence Assay. Cells seeded onto tissue culture chamber slides were transfected with plasmids as indicated. Twenty-four hours after transfection, the cells were fixed with cold acetone and incubated with primary antibody and subsequently with Alexa488- or Alexa568-labeled secondary antibodies. Mitochondria were stained by MitoTracker (Invitrogen). Cells were visualized using a confocal laser microscope (Fluoview FV10, Olympus).

BiFC Assay. Expression plasmids of NS4B, Cardif, or STING that was fused with N- or C-terminally truncated monomeric Kusabira-Green (mKG) were constructed by inserting polymerase chain reaction–amplified fragments encoding NS4B, Cardif, or STING, respectively, inserted into fragmented mKG vector (Coral Hue Fluo-Chase Kit; MBL). HEK293T cells were transfected with a complementary pair of mKG fusion plasmids. Twenty-four hours after transfection, fluorescence-positive cells were detected and counted by flow cytometry, or observed by confocal laser microscopy.

Small Interfering RNA Assay. Nucleotide sequences of STING-targeted small interfering RNAs (siRNAs) were as follows: (1) 5′-gcaacagcatctatgagcttctggagaac-3′, (2) 5′- gtgcagtgagccagcggctgtatattctc;-3′, (3) 5′-gctggcat ggtcatattacatcggatatc-3′.[22] Stealth RNAi Negative Control Duplex (Medium GC Duplex, Invitrogen) was used. Forty-eight hours after siRNA transfection, expression levels of STING were detected by immunoblotting.

Statistical Analyses. Statistical analyses were performed using unpaired, two-tailed Student t test. $P < 0.05$ were considered to be statistically significant.

Results

NS4B Suppressed RIG-I, Cardif, and STING-Mediated Activation of IFN-β Expression Signaling. First, we performed a reporter assay using a luciferase reporter plasmid regulated by native IFN-β promoter. Consistent with our previous study,[19] overexpression of NS4B, as well as NS3/4A, inhibited the IFN-β promoter activation that was induced by ΔRIG-I and Cardif, respectively (Fig. 1A). We next studied whether NS4B targets STING and inhibits RIG-I pathway–mediated activation of IFN-β production. Expression of NS4B protein significantly suppressed STING-mediated activation of the IFN-β promoter reporter, whereas expression of NS3/4A showed no effect on STING-induced IFN-β promoter activity (Fig. 1A). To study whether NS4B blocks the STING-mediated DNA-sensing pathway, we performed a reporter assay using a luciferase reporter plasmid cotransfection with poly(dA:dT), which is a synthetic analog of B-DNA and has been reported to induce STING-mediated IFN-β production and NS4B. NS4B significantly blocked poly(dA:dT)-induced IFN-β promoter activation, suggesting that NS4B may block STING signaling in the DNA-sensing pathway (Fig. 1A).

Activation of RIG-I signaling induces phosphorylation of IRF-3, which is a hallmark of IRF-3 activation.[32] Thus, we examined the effects of NS3/4A and NS4B expression on phosphorylation of IRF-3 by immunoblotting analysis. As shown in Fig. 1B, overexpression of ΔRIG-I, Cardif, or STING in HEK293T cells increased levels of phosphorylated IRF-3 (pIRF-3). Expression of NS4B impaired the IRF-3 phosphorylation that was induced by ΔRIG-I, Cardif, or STING. NS3/4A also blocked production of pIRF-3 induced by ΔRIG-I or Cardif. Intriguingly, NS3/4A did not block STING-induced pIRF-3 production. These results demonstrate that both NS3/4A and

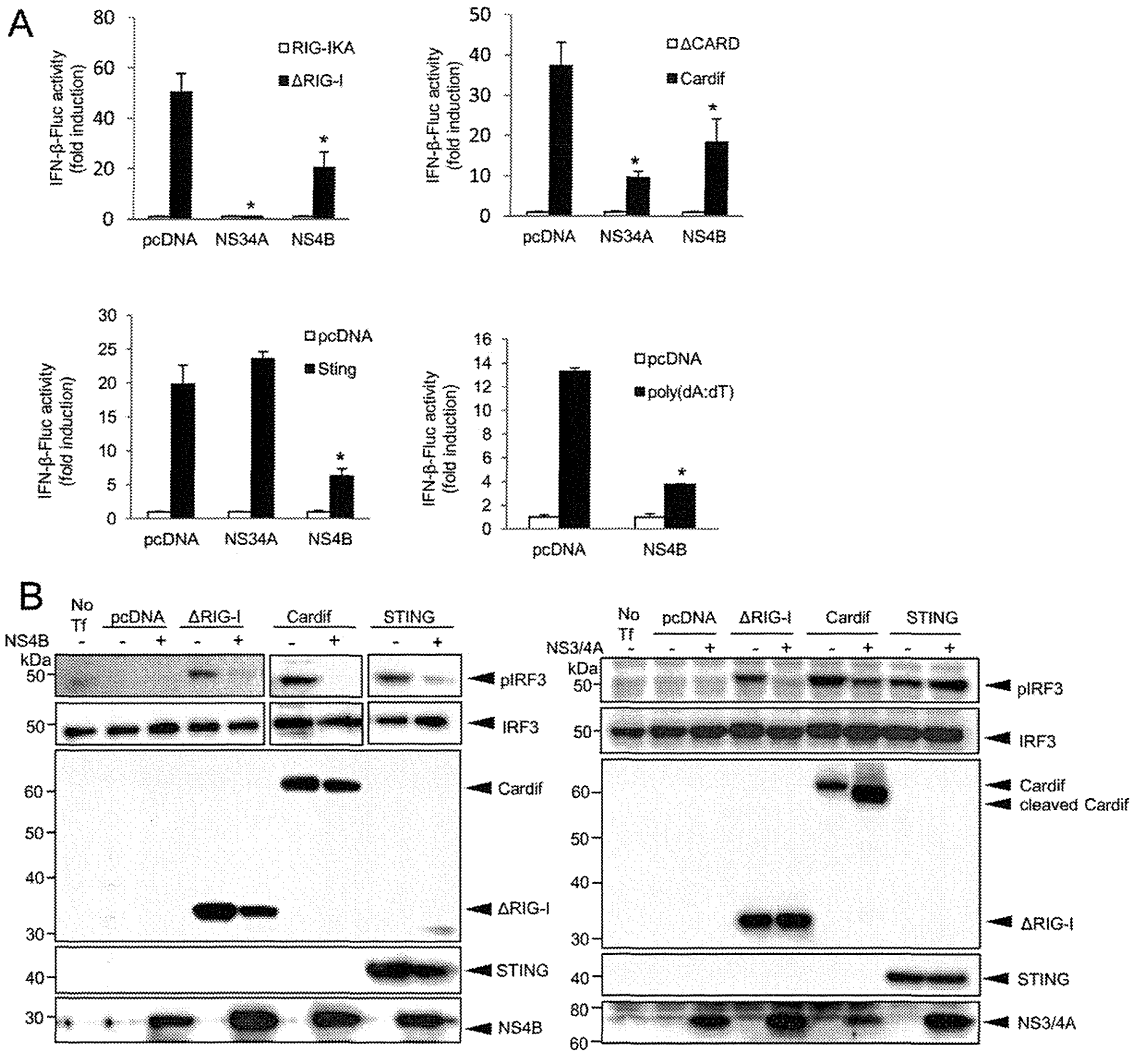

Fig. 1. NS4B suppressed IFN-β signaling mediated by RIG-I, Cardif, or STING. (A) Plasmids expressing ΔRIG-I, Cardif, or STING or poly(dA:dT) as well as NS3/4A or NS4B were cotransfected with pIFN-β-Fluc and pRL-CMV into HEK293T cells. After 24 hours, dual luciferase assays were performed. Plasmids expressing RIG-IKA, ΔCARD, or an empty plasmid (pcDNA) were used as a corresponding negative control. The experiments were performed more than three times and yielded consistent results. The *y* axis indicates relative IFN-β–Fluc activity. Assays were performed in triplicate and error bars indicate mean ± SD. $^*P < 0.05$. (B) HEK293T cells were cotransfected with indicated plasmids. On the day after transfection, the cells were lysed and immunoblot analyses were performed. No Tf, transfection-negative controls. pIRF-3 and IRF-3, phosphorylated and total IRF-3, respectively.

NS4B suppress RIG-I–mediated IFN-β production, but they do so by targeting different molecules in the signaling pathway.

Subcellular Localization of NS4B, Cardif, and STING. We next studied the subcellular localization of NS4B following its overexpression and measured the colocalization of NS4B with Cardif and STING in both HEK293T cells and Huh7 cells by indirect immunofluorescence microscopy. NS4B was localized predominantly in the ER, which is consistent with previous reports[33] (Fig. 2A). Cardif was localized in mitochondria but did not colocalize with the ER-resident host protein disulphide-isomerase (PDI). Interestingly, Cardif and NS4B colocalized partly at the boundary of the two proteins, although their original localization was different (Fig. 2A,C). STING was localized predominantly in the ER[20,21] (Fig. 2B,D). STING colocalized partly with Cardif, which is consistent with a previous report by Ishikawa and Barber[20] (Fig. 2B,D). In cells cotransfected with NS4B and STING expression plasmids, NS4B colocalized precisely with STING (Fig. 2B,D). To examine the region of NS4B-STING interaction, we next observed the two proteins by performing staining for them along with mitochondria-associated ER membrane (MAM), which is a physical association with mitochondria[34] and has been reported the site of Cardif-STING association.[24] Both NS4B and STING were adjacent to and partially colocalized

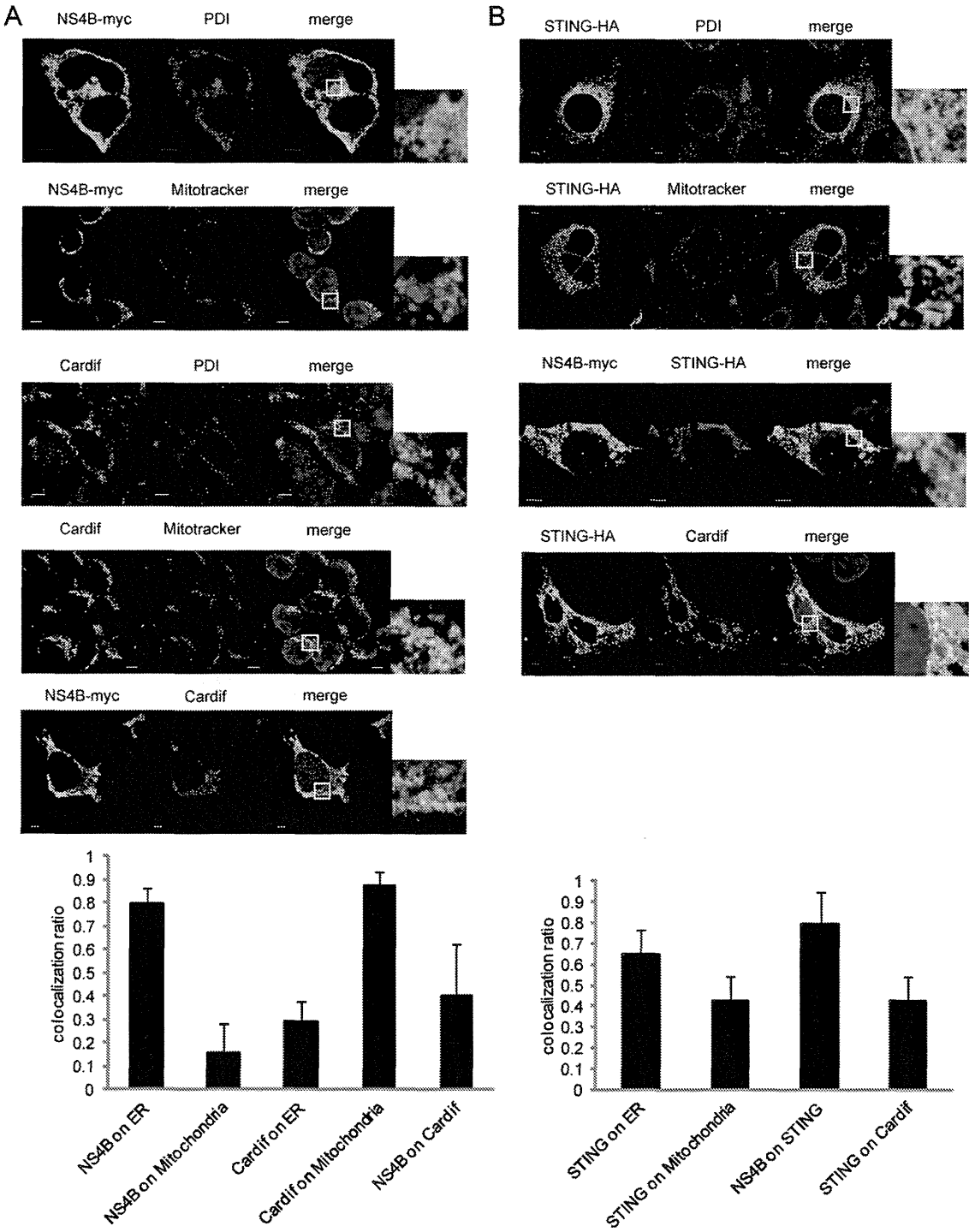

Fig. 2. Subcellular localization of NS4B, Cardif, and STING. (A-D) Subcellular localization of NS4B, Cardif, and STING in 293T (A,C) and Huh7 (B,D) cells. (A,C) NS4B-myc (first, second, and fifth panels of A and third panel of C) was transfected, and 24 hours later the cells were fixed and immunostained with anti-myc. In the third, fourth, and fifth panels of A, and the first and second panels of C, endogenous Cardif was detected with anti-Cardif antibody. ER was immunostained with anti-PDI antibody (first and third panels of A and first panel of C). Mitochondria were stained using Mitotracker (second and fourth panels of A and second panel of C). Nuclei were stained with 4',6-diamidino-2-phenylindole (DAPI). (B,D) STING-HA (all panels) and NS4B-myc (third panels) were transfected, and after 24 hours the cells were fixed and immunostained with anti-HA or anti-myc, respectively. In the fourth panels, endogenous Cardif was detected with anti-Cardif antibody. ER was immunostained with anti-PDI antibody (first panels). Mitochondria were stained using Mitotracker (second panels). Nuclei were stained with DAPI. (E) NS4B-myc and STING-HA were transfected into Huh7 cells and after 24 hours the cells were fixed and immunostained with anti-HA, anti-myc, and anti-FACL4 (MAM) antibody. Cells were visualized by confocal microscopy. Scale bars indicate 5 μm. In each microscopic image, the grade of protein colocalization in a single cell was quantified and is shown in the graphs at the bottom of each panel. Values are shown as the average colocalization ratio in 8 cells. Error bars indicate the mean + SD.

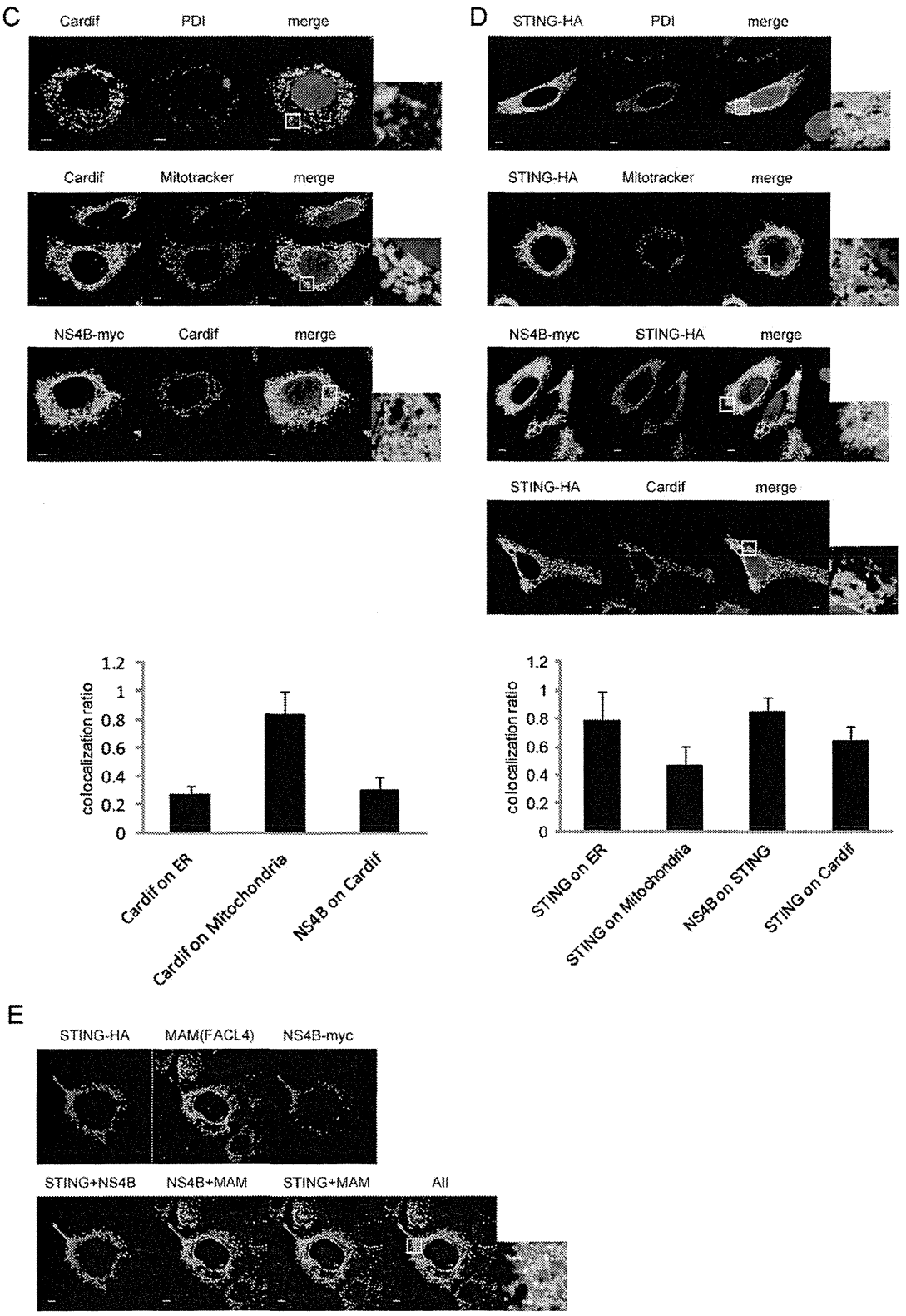

Fig. 2. Continued

with fatty acid-CoA ligase long chain 4 (FACL4), which is a MAM marker protein[35,36] (Fig. 2E). These findings suggest that NS4B might interact with STING on MAM more strongly than with Cardif.

Protein-Protein Interaction Between NS4B, Cardif, and STING. Knowing that NS4B was colocalized strongly with STING and only partly with Cardif, we next analyzed direct protein-protein interactions

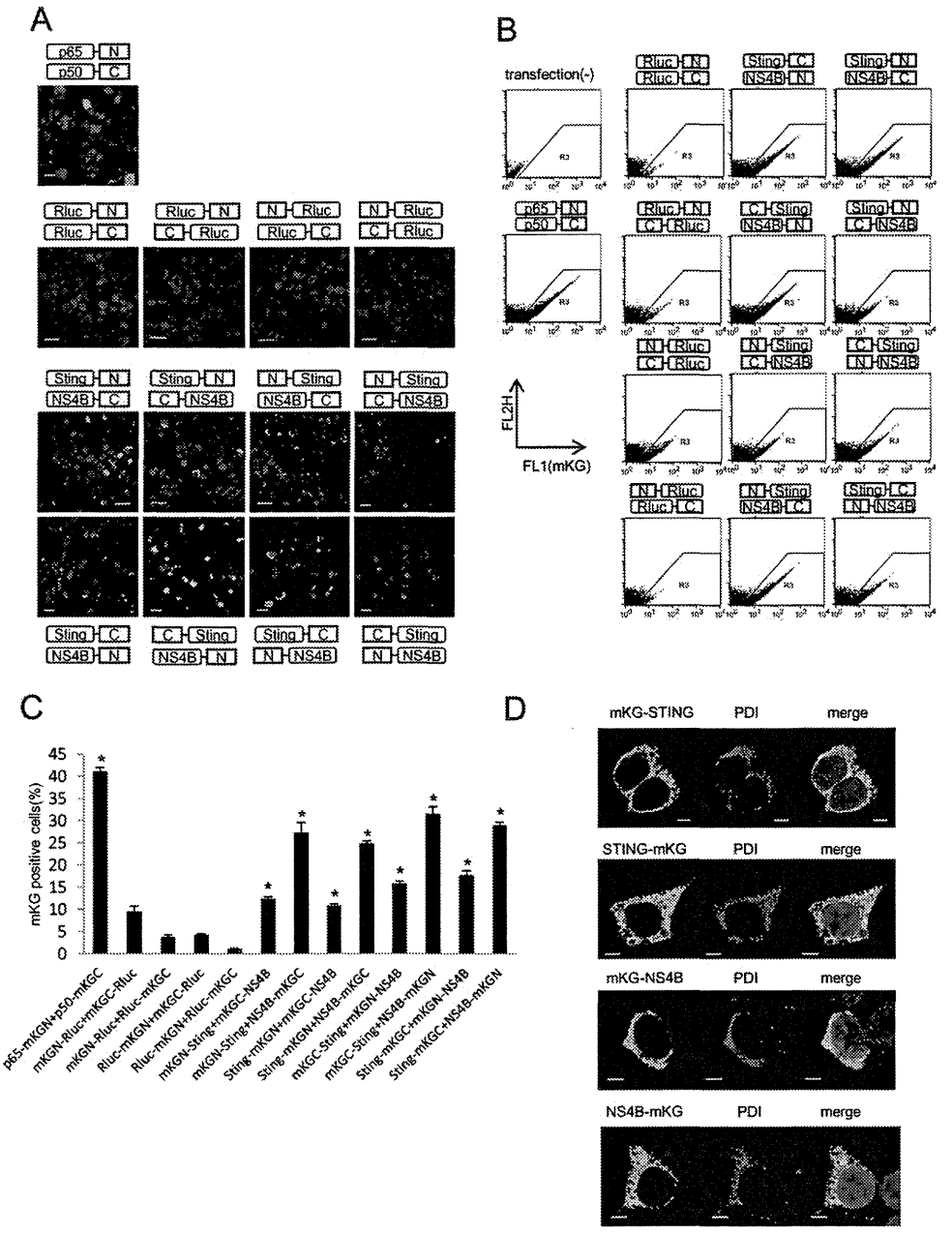

Fig. 3. BiFC assays of STING and NS4B. The complementary pairs of N- or C-terminally mKG-fused NS4B and STING expression plasmids were cotransfected in HEK293T cells. After 24 hours, the cells were fixed and observed by confocal microscopy (A) or subjected to flow cytometry to measure mKG-emitted fluorescence (BiFC signal) and to count BiFC signal-positive cells (B,C). Plasmids expressing p65-mKGN and p50-mKGC individually were used as a BiFC-positive control and plasmids expressing N- or C-terminally mKG fused Rluc were used as a negative control. The letters N and C denote complimentary N- and C-terminal fragments of mKG, respectively. Assays were performed in triplicate and error bars indicate the mean ± SD. Scale bars indicate 10 μm (A). *$P < 0.05$ compared with corresponding negative controls. (D) Plasmids expressing mKG fragment-fused STING or NS4B were transfected in HEK293T cells. After 24 hours, the cells were fixed and immunostained with anti-mKG and anti-PDI (ER) antibody. Nuclei were stained with DAPI. Cells were observed by confocal microscopy. Scale bars = 5 μm.

between NS4B, Cardif, and STING. To detect those interactions in living cells, we performed BiFC assays.[37,38] We constructed NS4B, Cardif, and STING expression plasmids that were N- or C-terminally fused with truncated mKG proteins, respectively. First, we cotransfected several different pairs of NS4B and STING expression plasmids that were fused with complementary pairs of N- or C-terminally truncated mKG. Strong fluorescence by mKG complexes (BiFC signal) was detected in all pairs of cotransfections, suggesting significant molecular interaction (Fig. 3A). In flow cytometry, all pairs of NS4B- and STING-mKG fusion proteins were positive for strong BiFC signal (Fig. 3B). The percentages of cells positive for BiFC signal were significantly higher in STING-mKG and NS4B-mKG fusion complexes than in corresponding controls (Fig. 3C). These results demonstrate that HCV-NS4B and STING proteins interact with each other strongly and specifically in cells. Fluorescence microscopy indicated that N- and C-terminal fusion of mKG onto NS4B and STING did not affect subcellular localization (Fig. 3D).

We next studied the molecular interaction between NS4B and Cardif by BiFC assay using NS4B and Cardif fusion plasmids that were tagged with complementary pairs of truncated mKG. Weak fluorescence was detected in cells transfected with the pairs N-Cardif and NS4B-C, N-Cardif and C-NS4B, C-Cardif and

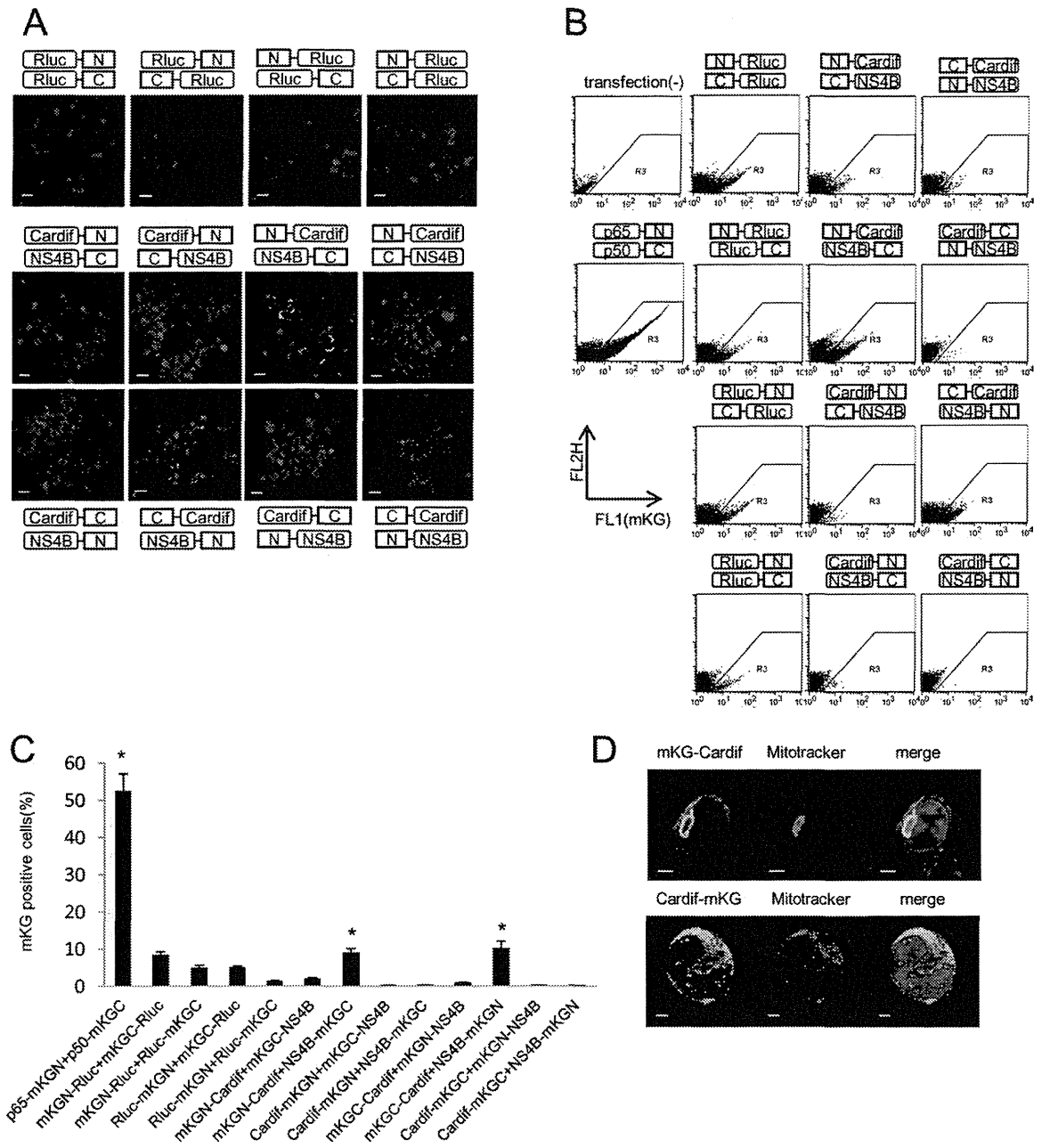

Fig. 4. BiFC assays of Cardif and NS4B. The complementary pairs of N- or C-terminally mKG-fused NS4B and Cardif expression plasmids were cotransfected in HEK293T cells. After 24 hours, the cells were fixed and observed by confocal microscopy (A) or subjected to flow cytometry to measure mKG-emitted fluorescence (BiFC signal) and to count BiFC signal-positive cells (B,C). Plasmids expressing p65-mKGN and p50-mKGC individually were used as a BiFC-positive control and plasmids expressing N- or C-terminally mKG-fused Rluc were used as a negative control. The letters N and C denote complimentary N- and C-terminal fragments of mKG, respectively. Assays were performed in triplicate, and error bars indicate the mean ± SD. Scale bars indicate 10 μm (A). *$P < 0.05$ compared with corresponding negative controls. (D) Plasmids expressing mKG fragment-fused STING or NS4B were transfected in HEK293T cells. After 24 hours, the cells were fixed and immunostained with anti-mKG antibody. Mitochondria were stained using Mitotracker, and nuclei were stained with DAPI. Cells were observed by confocal microscopy. Scale bars = 5 μm.

NS4B-N, and C-Cardif and N-NS4B (Fig. 4A,B). The percentage of cells positive for BiFC signal increased with the combination of N-Cardif and NS4B-C, and C-Cardif and NS4B-N (Fig. 4C). Fluorescence microscopy indicated that mKG-Cardif, but not Cardif-mKG, was partially colocalized with mitochondria, possibly due to disruption of mitochondria anchor domain by C-terminal fusion with mKG (Fig. 4D). These results indicate the lack of significant molecular interactions between NS4B and Cardif.

Binding of NS4B to STING Blocks Molecular Interaction Between Cardif and STING. It has been reported that STING binds Cardif directly.[20,22] Thus, we hypothesized that NS4B, through a competitive

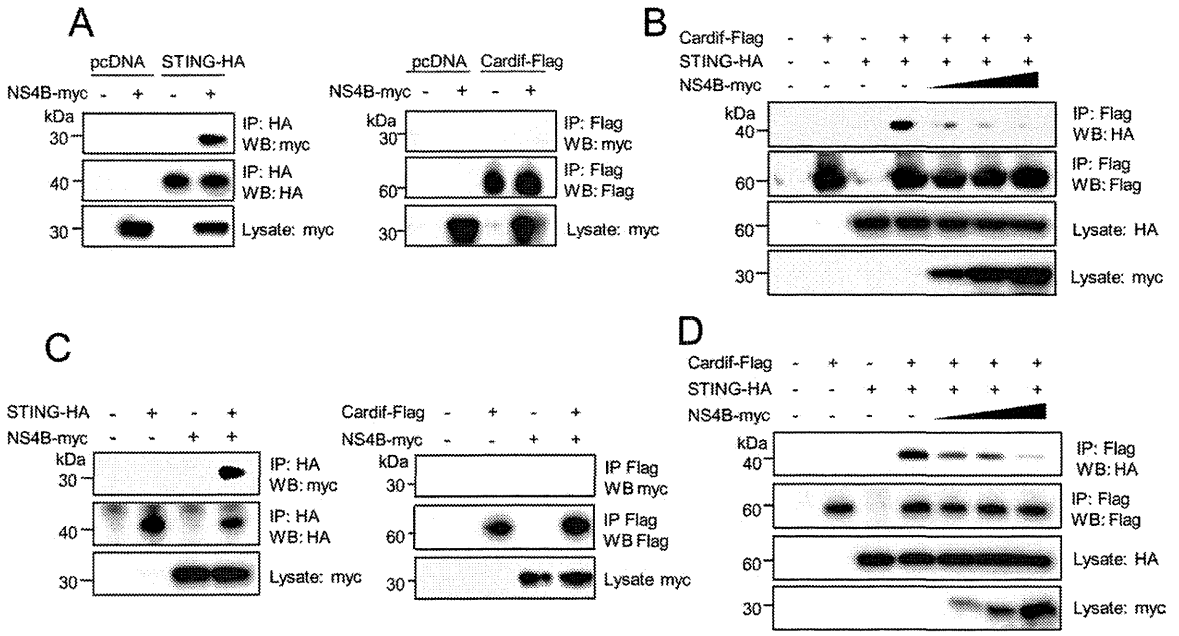

Fig. 5. Binding of NS4B to STING blocks molecular the interaction between Cardif and STING. (A,C) NS4B expression plasmid was cotransfected with STING or Cardif expression plasmid into HEK293T cells (A) or Huh7 cells (C). After 24 hours, cell lysates were subjected to immunoprecipitation using anti-HA or anti-Flag and were immunoblotted with anti-myc. (B,D) Cardif and STING expression plasmids were cotransfected with various amounts of NS4B plasmid in HEK293T cells (B) or Huh7 cells (D). After 24 hours, cells lysates were subjected to immunoprecipitation using anti-Flag and were immunoblotted with anti-HA.

interaction with STING, may hinder the direct molecular interaction between Cardif and STING. To verify this hypothesis, we performed immunoprecipitation assays. First, we transfected plasmids that expressed NS4B and Cardif, or NS4B and STING, in HEK293T cells or Huh7 cells, and performed immunoprecipitation. NS4B strongly bound to STING in both HEK293T cells and Huh7 cells, suggesting specific molecular interactions, whereas NS4B and Cardif did not show any obvious interaction (Fig. 5A,C). Consistent with previous reports, STING and Cardif showed significant interaction (Fig. 5B,D). Interestingly, those interactions were decreased by coexpression of NS4B, depending on its input amount, and finally blocked completely in both HEK293T and Huh7 cells (Fig. 5B,D). Collectively, the results above demonstrate that NS4B disrupts the interaction between Cardif and STING possibly through competitive binding to STING.

Effects on HCV Infection and Replication Levels by STING Knockdown and NS4B Overexpression. We next studied the impact of STING-mediated IFN production and its regulation by NS4B on HCV infection and cellular replication. First, we transfected three STING-targeted siRNAs into Huh7/Feo cells (Fig. 6A). As shown in Fig. 6B, STING knockdown cells conferred significantly higher permissibility to HCV replication. We next transfected HCV-JFH1 RNA into Huh7 cells that were transiently transfected with NS4B. As shown in Fig. 6C, HCV core protein expression was significantly higher in NS4B-overexpressed cells. Furthermore, HCV replication was increased significantly in Huh7/Feo cells overexpressing NS4B (Fig. 6D). Taken together, the results above demonstrate that STING and NS4B may negatively or positively regulate cellular permissiveness to HCV replication.

The N-terminal Domain of NS4B Is Essential for Suppressing IFN-β Promoter Activity Mediated by RIG-I, Cardif, and STING. It has been reported that the N-terminal domain of several forms of flaviviral NS4B shows structural homology with STING.[24] We therefore investigated whether the STING homology domain in NS4B is responsible for suppression of IFN-β production. We constructed two truncated NS4B expression plasmids, which covered the N terminus (NS4Bt1-84, amino acids 1 through 84) containing the STING homology domain and the C terminus (NS4Bt85-261, amino acids 85 through 261), respectively (Fig. 7A). Immunoblotting showed that NS4Bt1-84 and NS4Bt85-261 yielded protein bands of ~9 kDa and ~20 kDa, respectively. Aberrant bands in the truncated NS4B may be due to alternative posttranslational processing. HEK293T cells were transfected with ΔRIG-I, Cardif, or STING, and NS3/4A or the truncated NS4B, along with IFN-β-Fluc plasmid, and a reporter assay was performed. NS4Bt1-84 significantly suppressed RIG-I, Cardif, and STING-

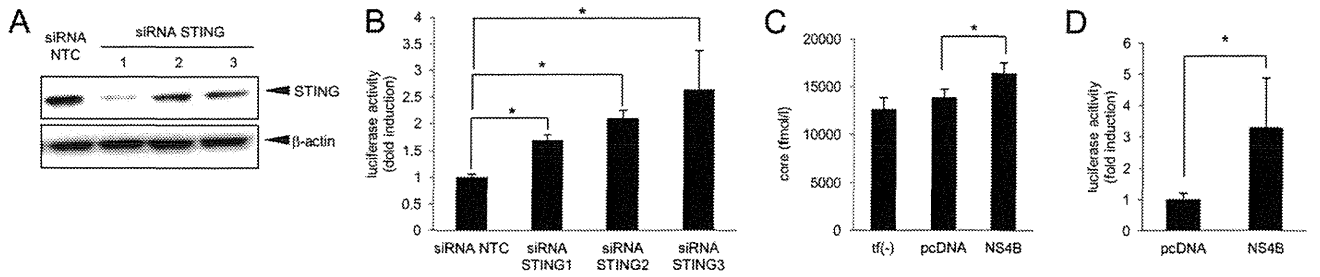

Fig. 6. Effects on HCV replication levels by STING knockdown and NS4B overexpression. (A) Effects of siRNA knockdown of STING by siRNA. Huh7 cells were transfected with STING-targeted siRNAs (siRNA STING-1, -2, and -3, respectively) or negative control siRNA (siRNA NTC). Seventy-two hours after transfection, cells were harvested and expression levels of STING protein were detected by immunoblotting. (B) Huh7 cells expressing HCV-Feo subgenomic replicon (Huh7/Feo)[27,28] were transfected with STING-targeted siRNAs or negative control siRNA. Seventy-two hours after transfection, cells were harvested, and internal luciferase activities were measured. The *y* axis indicates luciferase activity shown as a ratio of transfection-negative control. Assays were performed in triplicate, and error bars indicate the mean + SD. $*P < 0.05$ compared with corresponding negative controls. (C) Empty plasmid or plasmid expressing NS4B was transfected into Huh7 cells. After 24 hours, HCV-JFH1 RNA was transfected into these cells. Seventy-two hours after virus transfection, HCV core antigen levels in culture medium were measured. Assays were performed in triplicate, and error bars indicate the mean + SD. $*P < 0.05$ compared with corresponding negative controls. tf(−), transfection-negative control. (D) Huh7 cells expressing HCV-Feo replicon (Huh7/Feo)[27,28] were transfected with NS4B expressing plasmid or empty plasmid (pcDNA). Forty-eight hours after transfection, internal luciferase activities were measured. The *y* axis indicates luciferase activity shown as a ratio of the transfection-negative control. Assays were performed in triplicate, and error bars indicate the mean + SD. $*P < 0.05$ compared with corresponding negative controls.

induced IFN-β promoter activity, whereas NS4Bt85-261 did not (Fig. 7B). These results suggest that the N-terminal domain of NS4B is responsible for association with STING. Fluorescent microscopy indicated that both NS4Bt1-84 and NS4Bt85-26 colocalized with ER and STING (Fig. 7C).

NS4B Suppresses IFN Production Signaling Cooperatively with NS3/4A. It has been reported that

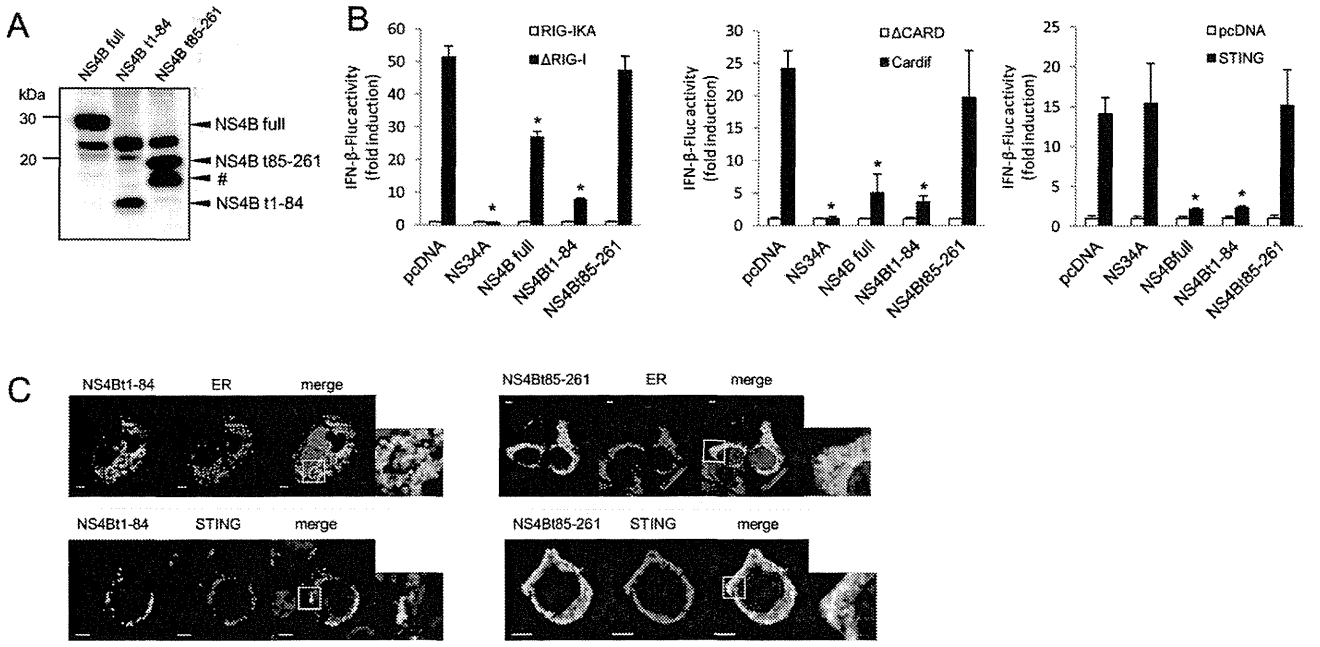

Fig. 7. The N-terminal domain of NS4B is essential for suppressing IFN-β promoter activity induced by RIG-I, Cardif, or STING. (A) Immunoblotting of NS4B and truncated NS4B, NS4B t1-84, and NS4Bt85-216. HEK293T cells were transfected with NS4B or truncated NS4B. After 24 hours, the cells were lysed and immunoblot assays were performed. The band indicated by the pound sign (#) is a truncated NS4B, probably generated via alternative posttranslational processing. (B) Plasmids expressing ΔRIG-I, Cardif, or STING as well as NS3/4A or the indicated truncated form of NS4B were cotransfected with pIFN-β-Fluc and pRL-CMV in HEK293T cells. Dual luciferase assays were performed 24 hours after transfection. Plasmids expressing RIG-IKA, ΔCARD, or pcDNA were used as negative controls. The *y* axis indicates IFN-β-Fluc activity shown as relative values. Assays were performed in triplicate, and error bars indicate the mean ± SD. $*P < 0.05$ compared with corresponding negative controls. (C) Plasmids expressing NS4Bt1-84-myc of NS4Bt85-261-myc were transfected with or without plasmids expressing HA-STING in HEK293T cells. After 24 hours, the cells were fixed and immunostained. Nuclei were stained with DAPI. Cells were observed by confocal microscopy. Scale bars indicate 5 μm.

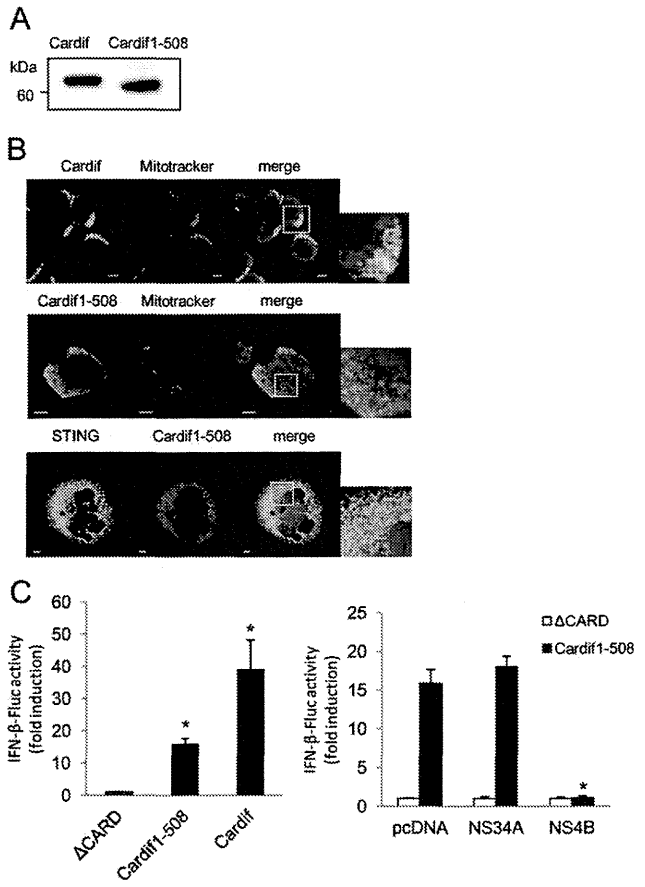

Fig. 8. NS4B suppressed IFN-β production pathway independently of and cooperatively with NS3/4A. (A) Immunoblotting of Cardif and truncated Cardif (Cardif1-508). HEK293T cells were transfected with Cardif or truncated Cardif (Cardif1-508). After 24 hours, the cells were lysed and immunoblot assays were performed. (B) Subcellular localization of Cardif and truncated Cardif (Cardif1-508). HEK293T cells were immunostained with anti-Cardif antibody or HEK293T cells were transfected with myc-tagged truncated Cardif (Cardif1-508-myc), and after 24 hours the cells were immunostained with anti-myc. Mitochondria were stained with Mitotracker (red) and nuclei were stained with DAPI (blue). Plasmid expressing myc-tagged truncated Cardif (Cardif1-508) and plasmid expressing HA-tagged STING were transfected into HEK293T cells. The cells were immunostained with anti-myc and anti-HA antibodies and analyzed by confocal laser microscopy. Scale bars = 10 μm. (C) Plasmids expressing Cardif or truncated Cardif (Cardif1-508) and pIFN-β-Fluc and pRL-CMV were transfected with or without plasmid expressing NS3/4A or NS4B into HEK293T cells as indicated. Dual luciferase assays were performed 24 hours after transfection. Plasmid expressing ΔCARD or pcDNA was used as a negative control. The *y* axis indicates IFN-β-Fluc activity shown as relative values. Assays were performed in triplicate, and error bars indicate the mean $\pm$ SD. $^*P < 0.05$.

HCV NS3/4A serine protease cleaves Cardif between Cys-508 and His-509, releases Cardif from the mitochondrial membrane, and blocks RIG-I–induced IFN-β production. We next assessed whether NS4B suppresses IFN-β production in the presence of Cardif cleaved by NS3/4A protease (Cardif1-508, Fig. 8A). The truncation of Cardif–C-terminal residue abolished mitochondrial localization but still colocalized with STING (Fig. 8B). The reporter assay showed that Cardif1-508 induced weak IFN-β activation. Interestingly, NS4B completely blocked the residual function of the Cardif1-508 protein to activate IFN-β expression, suggesting an additive effect of NS3/4A and NS4B on the RIG-I–activating pathway (Fig. 8C).

Discussion

It has been reported that viruses, including HCV, target IFN signaling to establish persistent replication in host cells.[39] We have reported that NS4B blocks the transcriptional activation of ISRE induced by overexpression of RIG-I and Cardif, but not by TBK1 or IKKϵ.[19] In the present study, we have shown that NS4B directly and specifically binds STING, an ER-residing scaffolding protein of Cardif and TBK1 and an inducer of IFN-β production (Figs. 3 and 5), and blocked the interaction between STING and Cardif (Fig. 5B,D) resulting in strong suppression of RIG-I–mediated phosphorylation of IRF-3 and expressional induction of IFN-β (Fig. 1). Furthermore, HCV replication was increased by knockdown of STING or overexpression of NS4B (Fig. 6). Taken together, our results demonstrate that HCV-NS4B strongly blocks virus-induced, RIG-I–mediated activation of IFN-β production signaling through targeting STING, which constitutes a novel mechanism of viral evasion from innate immune responses and establishment of persistent viral replication.

Our results also showed that the effects of NS4B on the RIG-I signaling were independent of NS3/4A-mediated cleavage of Cardif. Reporter assays showed that a cleaved form of Cardif (Cardif1-508) partially retained activity for the induction of IFN-β promoter activation. The residual IFN-β promoter activation was suppressed almost completely by NS4B but not by NS3/4A (Fig. 8C). These findings show that there are at least two mechanisms by which HCV can abrogate RIG-I–mediated IFN production signaling to accomplish abrogation of cellular antiviral responses.

NS4B and STING are ER proteins,[20,21,40] whereas Cardif is localized on the outer mitochondrial membrane.[9] Consistent with those reports, our immunostaining experiments demonstrated that most NS4B protein colocalized with STING (Fig. 2), and their association was localized on MAM (Fig. 2E). In addition to the significant colocalization of STING and NS4B, STING partially colocalized with Cardif at the boundary region of the two proteins (Fig. 2B). Furthermore, immunoprecipitation experiments showed that overexpression of NS4B completely blocked the interaction of STING with Cardif (Fig. 5B). Ishikawa et al.[24] reported

that STING could associate with Cardif by MAM interaction. Castanier et al.[41] reported that Cardif-STING interaction was enhanced in cells with elongated mitochondria. In addition, Horner et al.[42,43] observed NS3/4A targeting of MAM-anchored synapse and cleavage of Cardif at MAM but not in mitochondria. These results led us to speculate that interaction between STING and Cardif was enhanced by altering their subcellular localization during viral infection and that NS4B inhibits Cardif activation by interfering with the association between STING and Cardif on MAM-like NS3/4A behavior against host innate immunity.

HCV-NS4B is an ER-localized 27-kDa protein with several functions in the HCV life cycle. Cellular expression of NS4B induces convolution of the ER membrane and formation of a membranous web that harbors HCV replicase complex.[44,45] NS4B also has RNA-binding capacity.[46] In addition, several point mutations of NS4B were found to alter viral replication activity.[33,46,47] The studies above indicate that NS4B provides an important protein-protein or protein-RNA interaction platform within the HCV replication complex and is essential for viral RNA replication. However, there are few reports on the involvement of NS4B with antiviral immune responses. Consistent with our previous study, Moriyama et al.[48] reported that NS4B partially inhibited dsRNA-induced but not TRIF-induced activation of IFN-β. In NS4B-expressing cells, IFN-α induced activation of STAT1 was suppressed.[49] The present study has demonstrated that NS4B functions against the host IFN response, such that NS4B directly interacts with STING and suppresses downstream signaling, resulting in the induction of IFN production.

STING contains a domain homologous to the N terminus of NS4B derived from several flaviviruses, including HCV. In our previous NS4B truncation assay, the NS4B N-terminal domain (amino acids 1-110) was important for suppression of RIG-I–induced IFN-β expression.[19] Consistent with these results, N-terminally truncated NS4B (NS4Bt1-84) significantly suppressed STING and Cardif-induced IFN-β promoter activation, whereas the C terminus of NS4B (NS4Bt85-261) did not (Fig. 7). These results reinforce our hypothesis that NS4B binds STING at its homology domain and blocks the ability of STING to induce IFN-β production.

A small molecule inhibitor of NS4B has been developed and is under preliminary clinical trials.[50] Einav et al.[51] identified clemizole hydrochloride, an H1 histamine receptor antagonist, as an inhibitor of the RNA-binding function of NS4B and HCV RNA replication. A phase 1B clinical trial of clemizole in hepatitis C patients has been completed.[52] Other two NS4B inhibitors which are a compound of amiloride analog and anguizole are under preclinical development.[53,54] The possibility remains that such NS4B inhibitors may suppress HCV replication partly through inhibiting the ability of NS4B to suppress IFN-β production and restore cellular antiviral responses.

In conclusion, IFN production signaling induced by HCV infection and mediated by RIG-I is suppressed by NS4B through a direct interaction with STING. These virus-host interactions help to elucidate the mechanisms of persistent HCV infection and constitute a potential target to block HCV infection.

Acknowledgment: The authors are indebted to J. Tcshopp for providing Cardif, ΔCARD, and CARD and to G. N. Barber for the STING plasmids. This study was supported by grants from the Ministry of Education, Culture, Sports, Science and Technology, Japan; the Japan Society for the Promotion of Science; Ministry of Health, Labour and Welfare, Japan; and the Japan Health Sciences Foundation.

References

1. Samuel CE. Antiviral actions of interferons. Clin Microbiol Rev 2001; 14:778-809.
2. Taniguchi T, Takaoka A. The interferon-alpha/beta system in antiviral responses: a multimodal machinery of gene regulation by the IRF family of transcription factors. Curr Opin Immunol 2002;14:111-116.
3. Sakamoto N, Watanabe M. New therapeutic approaches to hepatitis C virus. J Gastroenterol 2009;44:643-649.
4. Bigger CB, Brasky KM, Lanford RE. DNA microarray analysis of chimpanzee liver during acute resolving hepatitis C virus infection. J Virol 2001;75:7059-7066.
5. Yoneyama M, Kikuchi M, Natsukawa T, Shinobu N, Imaizumi T, Miyagishi M, et al. The RNA helicase RIG-I has an essential function in duoble-stranded RNA-induced innate antiviral responses. Nat Immunol 2004;5:730-737.
6. Hornung V, Ellegast J, Kim S, Brzozka K, Jung A, Kato H, et al. 5'-Triphosphate RNA is the ligand for RIG-I. Science 2006;314:994-997.
7. Takahasi K, Yoneyama M, Nishihori T, Hirai R, Kumeta H, Narita R, et al. Nonself RNA-sensing mechanism of RIG-I helicase and activation of antiviral immune responses. Mol Cell 2008;29:428-440.
8. Kawai T. IPS-1, an adaptor triggering RIG-I- and Mda5-mediated type I interferon induction. Nat Immunol 2005;6:981-988.
9. Seth RB, Sun L, Ea CK, Chen ZJ. Identification and characterization of MAVS, a mitochondrial antiviral signaling protein that activates NF-κB and IRF 3. Cell 2005;122:669-682.
10. Xu LG. VISA is an adapter protein required for virus-triggered IFN-β signaling. Mol Cell 2005;19:727-740.
11. Meylan E, Curran J, Hofmann K, Moradpour D, Binder M, Bartenschlager R, et al. Cardif is an adaptor protein in the RIG-I antiviral pathway and is targeted by hepatitis C virus. Nature 2005;437: 1167-1172.
12. Yoneyama M, Suhara W, Fukuhara Y, Fukuda M, Nishida E, Fujita T. Direct triggering of the type I interferon system by virus infection: activation of a transcription factor complex containing IRF-3 and CBP/p300. EMBO J 1998;17:1087-1095.

13. Lin W, Kim SS, Yeung E, Kamegaya Y, Blackard JT, Kim KA, et al. Hepatitis C virus core protein blocks interferon signaling by interaction with the STAT1 SH2 domain. J Virol 2006;80:9226-9235.
14. Suda G, Sakamoto N, Itsui Y, Nakagawa M, Tasaka-Fujita M, Funaoka Y, et al. IL-6-mediated intersubgenotypic variation of interferon sensitivity in hepatitis C virus genotype 2a/2b chimeric clones. Virology 2010;407:80-90.
15. Funaoka Y, Sakamoto N, Suda G, Itsui Y, Nakagawa M, Kakinuma S, et al. Analysis of interferon signaling by infectious hepatitis C virus clones with substitutions of core amino acids 70 and 91. J Virol 2011; 85:5986-5994.
16. Loo YM, Owen DM, Li K, Erickson AK, Johnson CL, Fish PM, et al. Viral and therapeutic control of IFN-beta promoter stimulator 1 during hepatitis C virus infection. Proc Natl Acad Sci U S A 2006;103:6001-6006.
17. Li X-D, Sun L, Seth RB, Pineda G, Chen ZJ. Hepatitis C virus protease NS3/4A cleaves mitochondrial antiviral signaling protein off the mitochondria to evade innate immunity. Proc Natl Acad Sci U S A 2005; 102:17717-17722.
18. Baril M, Racine M-E, Penin F, Lamarre D. MAVS Dimer Is a Crucial Signaling Component of Innate Immunity and the Target of Hepatitis C Virus NS3/4A Protease. J. Virol. 2009;83:1299-1311.
19. Tasaka M, Sakamoto N, Itakura Y, Nakagawa M, Itsui Y, Sekine-Osajima Y, et al. Hepatitis C virus non-structural proteins responsible for suppression of the RIG-I/Cardif-induced interferon response. J Gen Virol 2007;88:3323-3333.
20. Ishikawa H, Barber GN. STING is an endoplasmic reticulum adaptor that facilitates innate immune signalling. Nature 2008;455:674-678.
21. Sun W, Li Y, Chen L, Chen H, You F, Zhou X, et al. ERIS, an endoplasmic reticulum IFN stimulator, activates innate immune signaling through dimerization. Proc Natl Acad Sci U S A 2009;106:8653-8658.
22. Zhong B, Yang Y, Li S, Wang YY, Li Y, Diao F, et al. The adaptor protein MITA links virus-sensing receptors to IRF3 transcription factor activation. Immunity 2008;29:538-550.
23. Jin L. MPYS, a novel membrane tetraspanner, is associated with major histocompatibility complex class II and mediates transduction of apoptotic signals. Mol Cell Biol 2008;28:5014-5026.
24. Ishikawa H, Ma Z, Barber GN. STING regulates intracellular DNA-mediated, type I interferon-dependent innate immunity. Nature 2009; 461:788-792.
25. Yanagi M, Purcell RH, Emerson SU, Bukh J. Transcripts from a single full-length cDNA clone of hepatitis C virus are infectious when directly trasfected into the liver of a chimpanzee. Proc Natl Acad Sci U S A 1997;94:8738-8743.
26. Lin R, Lacoste J, Nakhaei P, Sun Q, Yang L, Paz S, et al. Dissociation of a MAVS/IPS-1/VISA/Cardif-IKKepsilon molecular complex from the mitochondrial outer membrane by hepatitis C virus NS3-4A proteolytic cleavage. J Virol 2006;80:6072-6083.
27. Yokota T, Sakamoto N, Enomoto N, Tanabe Y, Miyagishi M, Maekawa S, et al. Inhibition of intracellular hepatitis C virus replication by synthetic and vector-derived small interfering RNAs. EMBO Rep 2003;4:602-608.
28. Tanabe Y, Sakamoto N, Enomoto N, Kurosaki M, Ueda E, Maekawa S, et al. Synergistic inhibition of intracellular hepatitis C virus replication by combination of ribavirin and interferon- alpha. J Infect Dis 2004;189:1129-1139.
29. Wakita T, Pietschmann T, Kato T, Date T, Miyamoto M, Zhao Z, et al. Production of infectious hepatitis C virus in tissue culture from a cloned viral genome. Nat Med 2005;11:791-796.
30. Lindenbach BD, Evans MJ, Syder AJ, Wolk B, Tellinghuisen TL, Liu CC, et al. Complete replication of hepatitis C virus in cell culture. Science 2005;309:623-626.
31. Nakagawa M, Sakamoto N, Enomoto N, Tanabe Y, Kanazawa N, Koyama T, et al. Specific inhibition of hepatitis C virus replication by cyclosporin A. Biochem Biophys Res Commun 2004;313:42-47.
32. Yamashiro T, Sakamoto N, Kurosaki M, Kanazawa N, Tanabe Y, Nakagawa M, et al. Negative regulation of intracellular hepatitis C virus replication by interferon regulatory factor 3. J Gastroenterol 2006;41:750-757.
33. Lindstrom H, Lundin M, Haggstrom S, Persson MA. Mutations of the hepatitis C virus protein NS4B on either side of the ER membrane affect the efficiency of subgenomic replicons. Virus Res 2006;121: 169-178.
34. Hayashi T, Rizzuto R, Hajnoczky G, Su TP. MAM: more than just a housekeeper. Trends Cell Biol 2009;19:81-88.
35. Lewin TM, Van Horn CG, Krisans SK, Coleman RA. Rat liver acyl-CoA synthetase 4 is a peripheral-membrane protein located in two distinct subcellular organelles, peroxisomes, and mitochondrial-associated membrane. Arch Biochem Biophys 2002;404:263-270.
36. Simmen T, Aslan JE, Blagoveshchenskaya AD, Thomas L, Wan L, Xiang Y, et al. PACS-2 controls endoplasmic reticulum-mitochondria communication and Bid-mediated apoptosis. EMBO J 2005;24:717-729.
37. Kerppola TK. Design and implementation of bimolecular fluorescence complementation (BiFC) assays for the visualization of protein interactions in living cells. Nat Protoc 2006;1:1278-1286.
38. Kerppola TK. Bimolecular fluorescence complementation (BiFC) analysis as a probe of protein interactions in living cells. Annu Rev Biophys 2008;37:465-487.
39. Kato H. Differential roles of MDA5 and RIG-I helicases in the recognition of RNA viruses. Nature 2006;441:101-105.
40. Saitoh T, Fujita N, Hayashi T, Takahara K, Satoh T, Lee H, et al. Atg9a controls dsDNA-driven dynamic translocation of STING and the innate immune response. Proc Natl Acad Sci U S A 2009;106: 20842-20846.
41. Castanier C, Garcin D, Vazquez A, Arnoult D. Mitochondrial dynamics regulate the RIG-I-like receptor antiviral pathway. EMBO Rep 2009;11:133-138.
42. Horner SM, Liu HM, Park HS, Briley J, Gale M. Mitochondrial-associated endoplasmic reticulum membranes (MAM) form innate immune synapses and are targeted by hepatitis C virus. Proc Natl Acad Sci U S A 2011;108:14590-14595.
43. Horner SM, Park HS, Gale M Jr. Control of innate immune signaling and membrane targeting by the hepatitis C virus NS3/4A protease are governed by the NS3 helix α0. J Virol 2012;86:3112-3120.
44. Egger D, Wolk B, Gosert R, Bianchi L, Blum HE, Moradpour D, et al. Expression of Hepatitis C virus proteins induces distinct membrane alterations including a candidate viral replication complex. J Virol 2002;76:5974-5984.
45. Gretton SN, Taylor AI, McLauchlan J. Mobility of the hepatitis C virus NS4B protein on the endoplasmic reticulum membrane and membrane-associated foci. J Gen Virol 2005;86:1415-1421.
46. Einav S, Elazar M, Danieli T, Glenn JS. A nucleotide binding motif in hepatitis C virus (HCV) NS4B mediates HCV RNA replication. J Virol 2004;78:11288-11295.
47. Elazar M, Liu P, Rice CM, Glenn JS. An N-terminal amphipathic helix in hepatitis C virus (HCV) NS4B mediates membrane association, correct localization of replication complex proteins, and HCV RNA replication. J Virol 2004;78:11393-11400.
48. Moriyama M, Kato N, Otsuka M, Shao RX, Taniguchi H, Kawabe T, et al. Interferon-beta is activated by hepatitis C virus NS5B and inhibited by NS4A, NS4B, and NS5A. Hepatol Int 2007;1:302-310.
49. Xu J, Liu S, Xu Y, Tien P, Gao G. Identification of the nonstructural protein 4B of hepatitis C virus as a factor that inhibits the antiviral activity of interferon-alpha. Virus Res 2009;141:55-62.
50. Hofmann WP, Zeuzem S. A new standard of care for the treatment of chronic HCV infection. Nat Rev Gastroenterol Hepatol 2011;8: 257-264.
51. Einav S, Gerber D, Bryson PD, Sklan EH, Elazar M, Maerkl SJ, et al. Discovery of a hepatitis C target and its pharmacological inhibitors by microfluidic affinity analysis. Nat Biotech 2008;26:1019-1027.
52. Rai R, Deval J. New opportunities in anti-hepatitis C virus drug discovery: targeting NS4B. Antiviral Res 2011;90:93-101.
53. Cho NJ, Dvory-Sobol H, Lee C, Cho SJ, Bryson P, Masek M, et al. Identification of a class of HCV inhibitors directed against the nonstructural protein NS4B. Sci Transl Med 2010;2:15ra16.
54. Bryson PD, Cho NJ, Einav S, Lee C, Tai V, Bechtel J, et al. A small molecule inhibits HCV replication and alters NS4B's subcellular distribution. Antiviral Res 2010;87:1-8.

AAC
Journals.ASM.org

Identification of Novel *N*-(Morpholine-4-Carbonyloxy) Amidine Compounds as Potent Inhibitors against Hepatitis C Virus Replication

Akiko Kusano-Kitazume,[a] Naoya Sakamoto,[a,b] Yukiko Okuno,[c] Yuko Sekine-Osajima,[a] Mina Nakagawa,[a,b] Sei Kakinuma,[a,b] Kei Kiyohashi,[a] Sayuri Nitta,[a] Miyako Murakawa,[a] Seishin Azuma,[a] Yuki Nishimura-Sakurai,[a] Masatoshi Hagiwara,[c] and Mamoru Watanabe[a]

Department of Gastroenterology and Hepatology[a] and Department for Hepatitis Control,[b] Tokyo Medical and Dental University, Tokyo, Japan, and Department of Anatomy and Developmental Biology, Graduate School of Medicine, Kyoto University, Kyoto, Japan[c]

To identify novel compounds that possess antiviral activity against hepatitis C virus (HCV), we screened a library of small molecules with various amounts of structural diversity using an HCV replicon-expressing cell line and performed additional validations using the HCV-JFH1 infectious-virus cell culture. Of 4,004 chemical compounds, we identified 4 novel compounds that suppressed HCV replication with 50% effective concentrations of ranging from 0.36 to 4.81 μM. *N*′-(Morpholine-4-carbonyloxy)-2-(naphthalen-1-yl) acetimidamide (MCNA) was the most potent and also produced a small synergistic effect when used in combination with alpha interferon. Structure-activity relationship (SAR) analyses revealed 4 derivative compounds with antiviral activity. Further SAR analyses revealed that the *N*-(morpholine-4-carbonyloxy) amidine moiety was a key structural element for antiviral activity. Treatment of cells with MCNA activated nuclear factor κB and downstream gene expression. In conclusion, *N*-(morpholine-4-carbonyloxy) amidine and other related morpholine compounds specifically suppressed HCV replication and may have potential as novel chemotherapeutic agents.

Hepatitis C virus (HCV) is a major human pathogen. It is associated with persistent liver infection, which leads to the development of chronic hepatitis, liver cirrhosis, and hepatocellular carcinoma (13). Treatment with pegylated interferon (IFN) and ribavirin is associated with significant side effects and is effective in only half the patients infected with HCV genotype 1 (6). More effective and more tolerable therapeutics are under development, and direct-acting antiviral agents (DAAs) for HCV infection are currently in advanced clinical trials. In combination with IFN and ribavirin, the HCV protease inhibitors telaprevir and boceprevir have recently been approved for treatment of genotype 1 HCV infection in the United States, Canada, Europe, and Asian countries (11, 12, 22). Although these two drugs can achieve higher sustained virologic response rates than IFN and ribavirin, their effects could be compromised by the emergence of highly prevalent drug-resistant mutants (25). Thus, it is crucial to use several different classes of DAAs in combination to improve efficacy and reduce viral breakthrough.

The HCV subgenomic replicon system has been widely used to screen compound libraries for inhibitors of viral replication, using reporter activity as a surrogate marker for HCV replication. We previously reported the successful adaptation of the Huh7/Rep-Feo replicon cell line to a high-throughput screening assay system (28). This approach contributed to the discovery of antiviral compounds, such as hydroxyl-methyl-glutaryl coenzyme A reductase inhibitors (10) and epoxide compounds (20). In our present study, we used the Huh7/Rep-Feo replicon cell line to screen a library of small molecules with various amounts of structural diversity to identify novel compounds possessing antiviral activity against HCV. We showed that the screening hit compounds inhibited HCV replication in an HCV genotype 2a (JFH-1) infectious-virus cell culture (29). The most potent compound was *N*′-(morpholine-4-carbonyloxy)-2-(naphthalen-1-yl) acetimidamide (MCNA). Structure-activity relationship (SAR) analyses revealed that the *N*-(morpholine-4-carbonyloxy) amidine moiety was a key structural element for antiviral activity. We also investigated the possible mechanisms of action of these compounds and showed that MCNA likely inhibited HCV replication through activation of the nuclear factor κB (NF-κB) pathway.

MATERIALS AND METHODS

Reagents and chemicals. Recombinant human alpha 2b interferon (IFN-α2b) was obtained from Schering-Plough (Kenilworth, NJ), the NS3/4A protease inhibitor BILN 2061 from Boehringer Ingelheim (Ingelheim, Germany), beta-mercaptoethanol from Wako (Osaka, Japan), and recombinant human tumor necrosis factor alpha (TNF-α) from Sigma (St. Louis, MO). The library of chemicals that were screened was provided by the Chemical Biology Screening Center at Tokyo Medical and Dental University. Information about the library is available at http://bsmdb.tmd.ac.jp. The important features of the library were the abundance of pharmacophores and the great diversity. Lipinski's rule of five was used to evaluate drug similarity (15). The purity of each chemical from the library was greater than 90%. For SAR analyses, 27 compounds were purchased from Assinex (Moscow, Russia), ChemBridge (San Diego, CA), ChemDiv (San Diego, CA), Enamine (Kiev, Ukraine), Maybridge (Cambridge, United Kingdom), Ramidus AB (Lund, Sweden), SALOR (St. Louis, MO), Scientific Exchange (Center Ossipee, NH), or Vitas-M (Moscow, Russia). The chemicals were all prepared at concentrations of 10 mM in dimethyl sulfoxide (Sigma) and stored at −20°C until they were used.

Cell lines and cell culture maintenance. Huh7 and Huh7.5.1 cell lines (32) were maintained in Dulbecco's modified Eagle's medium (Sigma)

Received 22 September 2011 Returned for modification 18 October 2011
Accepted 14 December 2011
Published ahead of print 27 December 2011
Address correspondence to Naoya Sakamoto, nsakamoto.gast@tmd.ac.jp.
A. Kusano-Kitazume and N. Sakamoto contributed equally to this work.
Supplemental material for this article may be found at http://aac.asm.org/.

doi:10.1128/AAC.05764-11

supplemented with 10% fetal bovine serum and incubated at 37°C under 5% CO_2. The maintenance medium for the HCV replicon-harboring cell line, Huh7/Rep-Feo, was supplemented with 500 μg/ml of G418 (Nacalai Tesque, Kyoto, Japan).

HCV replicon construction and cell culture. An HCV subgenomic replicon plasmid that contained Rep-Feo, pHC1bneo/delS (Rep-Feo-1b), was derived from the HCV-N strain. RNA was synthesized from pRep-Feo and transfected into Huh7 cells. After culture in the presence of G418, a cell line that stably expressed the replicon was established (28, 31).

Cell-based screening of antiviral activity. Huh7/Rep-Feo cells were seeded at a density of 4,000 cells/well in 100 μl of medium in 96-well plates and incubated for 24 h. Test compound solutions, 10 mM in 100% dimethyl sulfoxide (DMSO), were added to the wells; for primary screening, the final concentration was 5 μM. The assay plates were incubated as described above for another 48 h, and luciferase activity was measured with a luminometer (Perkin-Elmer) using the Bright-Glo Luciferase assay system (Promega) following the manufacturer's instructions. Assays were performed in triplicate, and the results were expressed as means and standard deviations (SD) as percentages of the controls. Compounds were considered hits if they inhibited >50% of the mean control luciferase activities. Compounds were considered cytotoxic if they reduced cell viability below 70% of the control in dimethylthiazol carboxymethoxyphenyl sulfophenyl tetrazolium (MTS) assays and were discarded. The hit compounds were then validated by secondary screening, which determined the antiviral activities of each compound serially diluted at concentrations ranging from 0.1 μM to 30 μM under Huh7/Rep-Feo cells cultured in an identical manner to the primary screen. Compounds inhibiting replication with a 50% effective concentration (EC_{50}) of <5 μM and a selectivity index (SI) of >5 were selected for further analysis.

MTS assay. To evaluate cell viability, MTS assays were performed using the CellTiter 96 Aqueous One Solution Cell Proliferation Assay (Promega) according to the manufacturer's directions.

Calculation of the EC_{50}, CC_{50}, and SI. The EC_{50} indicates the concentration of test compound that inhibits replicon-based luciferase activity by 50%. The 50% cytotoxic concentration (CC_{50}) indicates the concentration that inhibits cell viability by 50%. The EC_{50} and CC_{50} values were calculated using probit regression analysis (2, 26). The selectivity index was calculated by dividing the CC_{50} by the EC_{50}.

Reporter and expression plasmids. The plasmid pC1neo-Rluc-IRES-Fluc was constructed to analyze the HCV internal ribosome entry site (IRES)-mediated translation efficiency (19). The plasmid expressed a bicistronic mRNA containing the *Renilla* luciferase gene translated in a cap-dependent manner, and firefly luciferase was translated by HCV-IRES-mediated initiation. The plasmid pISRE-TA-Luc (Invitrogen, Carlsbad, CA) expressed the firefly luciferase reporter gene under the control of the interferon stimulation response element (ISRE). The plasmid pNF-κB-TA-Luc (Clontech Laboratories, Franklin Lakes, NJ) expressed the firefly luciferase reporter gene under the control of NF-κB. The plasmid pRL-CMV (Promega, Madison, WI), which expressed the *Renilla* luciferase gene under the control of the cytomegalovirus early promoter/enhancer, was used as a control for the transfection efficiency of pISRE-TA-Luc and pNF-κB-TA-Luc (8).

Western blot analysis. Fifteen micrograms of total cell lysates was separated using NuPage 4-to-12% Bis-Tris gels (Invitrogen) and blotted onto polyvinylidene difluoride membranes. Each membrane was incubated with primary antibodies followed by a peroxidase-labeled anti-IgG antibody and visualized by chemiluminescence reaction using the ECL Western Blotting Analysis System (Amersham Biosciences, Buckinghamshire, United Kingdom). The primary antibodies were anti-NS5A (BioDesign, Saco, ME), anti-HCV core (kindly provided by T. Wakita), anti-phospho-p65 (Ser536) (93H1; Cell Signaling Technology, Beverly, MA), anti-IκBα (Santa Cruz Biotechnology, Santa Cruz, CA), and anti-β-actin (Sigma) antibodies.

HCV-JFH1 virus cell culture. HCV-JFH1 RNA transcribed *in vitro* was transfected into Huh7.5.1 cells. The transfected cells were subcultured every 3 to 5 days. The culture supernatant was subsequently transferred onto Huh7.5.1 cells.

TABLE 1 Effects of the leading hit compounds on HCV replication[a]

Compound	EC_{50} (μM)	CC_{50} (μM)	SI
1	0.36 (0.22–0.58)	45.2 (35.9–56.9)	126
2	0.86 (0.73–1.02)	>100	>116
3	0.94 (0.76–1.06)	25.3 (19.8–32.3)	26.9
4	4.81 (3.79–6.12)	27.1 (17.1–58.0)	5.64

[a] The EC_{50} and CC_{50} values are reported, with 95% confidence intervals in parentheses, from a representative experiment performed in triplicate.

Real-time RT-PCR analysis. The protocols and primers for real-time RT-PCR analysis of HCV RNA have been described previously (17). Briefly, total cellular RNA was isolated using an RNeasy Minikit (Qiagen, Valencia, CA), reverse transcribed, and subjected to real-time RT-PCR analysis. Expression of mRNA was quantified using the TaqMan Universal PCR Master Mix (Applied Biosystems, Foster City, CA) and the ABI 7500 real-time PCR system (Applied Biosystems).

Analyses of drug synergism. The effects on HCV replication of antiviral hit compounds plus IFN-α or BILN 2061 were analyzed according to classical isobologram analyses (24, 28). Dose-inhibition curves for IFN or BILN 2061 and the test compounds were drawn, with the 2 drugs (IFN or BILN 2061 and each test compound) used alone or in combination. For each drug combination, the concentrations of IFN or BILN 2061 and test compound that inhibited HCV replication by 50% (EC_{50}s) were plotted against the fractional concentration of IFN or BILN 2061 and the compound on the *x* and *y* axes, respectively. A theoretical line of additivity was drawn between plots of the EC_{50}s obtained for either drug used alone. The combined effects of the 2 drugs were considered to be additive, synergistic, or antagonistic if the plots of the combined drugs were located on, below, or above the line of additivity, respectively.

Statistical analyses. Statistical analyses were performed using Welch's *t* test. *P* values of less than 0.01 were considered statistically significant.

RESULTS

Screening results. To identify novel regulators of HCV replication, 4,004 chemical compounds were screened using the Huh7/Rep-Feo replicon assay system. The primary screens identified 117 compounds that inhibited ≥50% of replicon luciferase activity at 5 μM. Of the 117 compounds, 74 were cytotoxic and could not be further evaluated. In the secondary screen, nontoxic primary hits were evaluated by determining the antiviral activities of serial dilutions at concentrations ranging from 0.1 μM to 30 μM. This screen identified 19 compounds with EC_{50}s of less than 5 μM and CC_{50} values 5-fold greater than the EC_{50} values. The effect of each secondary hit on HCV-NS5A protein expression was examined using Western blot analysis. Of the 19 compounds, 4 compounds, designated 1, 2, 3, and 4, suppressed HCV subgenomic replication, with EC_{50}s ranging from 0.36 to 4.81 μM and SIs ranging from 5.64 to more than 100 (Table 1 and Fig. 1A and B; see Table S1 in the supplemental material). By Western blot analysis, compounds 1, 2, and 3 decreased HCV-NS5A protein levels at concentrations of 5 μM after incubation for 48 h (Fig. 1C). Compared with compounds 1, 2, and 3, the effect of compound 4 on HCV-NS5A protein expression was not remarkable at a concentration of 5 μM, similar to the results from the luciferase assay shown in Fig. 1B. The effects of the compounds on the HCV replicon were further validated in the JFH-1 cell culture. As shown in Fig. 1D, compounds 1, 2, 3, and 4 significantly inhibited intracellular RNA replication of HCV-JFH1. Although compound 4 was negative by Western blot analysis, it decreased HCV replication in the other